Kaon mixing beyond the SM from $N_f = 2$ tmQCD and model independent constraints from the UTA

The ETM collaboration

V. Bertone,[a] **N. Carrasco,**[b] **M. Ciuchini,**[c] **P. Dimopoulos,**[d] **R. Frezzotti,**[d,e]
V. Giménez,[b] **V. Lubicz,**[f,c] **G. Martinelli,**[g,h] **F. Mescia,**[i] **M. Papinutto,**[j,k,1]
G.C. Rossi,[d,e] **L. Silvestrini,**[h] **S. Simula,**[c] **C. Tarantino**[f,c] **and A. Vladikas**[e]

[a]*Physikalisches Institut, Albert-Ludwigs-Universität Freiburg,*
 Hermann-Herder-Straße 3, D-79104 Freiburg i. B., Germany

[b]*Departament de Física Teòrica and IFIC, Universitat de València-CSIC,*
 Dr. Moliner 50, E-46100 València, Spain

[c]*INFN, Sezione di Roma Tre, c/o Dipartimento di Fisica, Università Roma Tre,*
 Via della Vasca Navale 84, I-00146 Rome, Italy

[d]*Dipartimento di Fisica, Università di Roma "Tor Vergata",*
 Via della Ricerca Scientifica 1, I-00133 Rome, Italy

[e]*INFN, Sezione di "Tor Vergata", c/o Dipartimento di Fisica,*
 Università di Roma "Tor Vergata",
 Via della Ricerca Scientifica 1, I-00133 Rome, Italy

[f]*Dipartimento di Fisica, Università Roma Tre,*
 Via della Vasca Navale 84, I-00146 Rome, Italy

[g]*Scuola Internazionale Superiore di Studi Avanzati (SISSA),*
 Via Bonomea 265, 34136 Trieste, Italy

[h]*NFN, Sezione di Roma,*
 Piazzale A. Moro, I-00185 Rome, Italy

[i]*Departament d'Estructura i Constituents de la Matèria,*
 and Institut de Ciències del Cosmos, Universitat de Barcelona,
 6a planta, Diagonal 647, E-08028 Barcelona, Spain

---

[1]On leave of absence from Dipartimento di Fisica, Università di Roma "La Sapienza" Piazzale A. Moro, I-00185 Rome, Italy.

^{j} *Laboratoire de Physique Subatomique et de Cosmologie, UJF/CNRS-IN2P3/INPG,*
  53 rue des Martyrs, 38026 Grenoble, France

^{k} *Departamento de Física Teórica and Instituto de Física Teórica UAM/CSIC,*
  Universidad Autónoma de Madrid,
  Cantoblanco E-28049 Madrid, Spain

  E-mail: valerio.bertone@cern.ch, nuria.carrasco@uv.es,
  ciuchini@roma3.infn.it, dimopoulos@roma2.infn.it,
  Roberto.Frezzotti@roma2.infn.it, vicente.gimenez@uv.es,
  lubicz@fis.uniroma3.it, guido.martinelli@sissa.it, mescia@ub.edu,
  mauro.papinutto@roma1.infn.it, giancarlo.rossi@roma2.infn.it,
  Luca.Silvestrini@roma1.infn.it, silvano.simula@roma3.infn.it,
  tarantino@fis.uniroma3.it, tassos.vladikas@roma2.infn.it

ABSTRACT: We present the first unquenched, continuum limit, lattice QCD results for the matrix elements of the operators describing neutral kaon oscillations in extensions of the Standard Model. Owing to the accuracy of our calculation on $\Delta S = 2$ weak Hamiltonian matrix elements, we are able to provide a refined Unitarity Triangle analysis improving the bounds coming from model independent constraints on New Physics. In our non-perturbative computation we use a combination of $N_f = 2$ maximally twisted sea quarks and Osterwalder-Seiler valence quarks in order to achieve both O(a)-improvement and continuum-like renormalization properties for the relevant four-fermion operators. The calculation of the renormalization constants has been performed non-perturbatively in the RI-MOM scheme. Based on simulations at four values of the lattice spacing and a number of quark masses we have extrapolated/interpolated our results to the continuum limit and physical light/strange quark masses.

KEYWORDS: Lattice QCD, Beyond Standard Model

Contents

1 Introduction

The fundamental target of present-day research activity in Particle Physics is the search for New Physics (NP) effects beyond the Standard Model (SM) predictions. Two main routes are followed, one based on the study of processes in which the direct production of NP particles at high energy colliders like the LHC takes place, and a second one based on the indirect investigation of NP effects coming from the exchange of virtual NP particles.

In the so-called indirect approach a crucial role is played by Flavor Physics processes that are sensitive to NP through loop effects. These processes vanish at tree level in the SM, and some of them are theoretically very clean, despite the fact that they are loop mediated, and in some cases also CKM or helicity suppressed. Among them, $\Delta F = 2$ transitions have always provided some of the most stringent constraints on NP. For instance, the constraints from $K^0 - \bar{K}^0$ oscillations are particularly stringent for NP models that generate transitions between quarks of different chiralities [1]–[4]. Therefore, an accurate determination of the $\Delta S = 2$ bag parameters (B-parameters) is crucial to the improvement of NP constraints.

In the present work, we provide the first accurate lattice determination of the $\Delta S = 2$ B-parameters relevant for physics beyond the SM, calculated in the continuum limit and using data from unquenched, $N_f = 2$, dynamical quark simulations.[1] Our results represent a significant improvement with respect to the (quenched) input values of refs. [6] and [7] used so far in phenomenological analyses. The calculation of the B_K parameter that is relevant for the $K^0 - \bar{K}^0$ mixing in the SM has been presented in [8] using three values of the lattice spacing. In the present work we update that value by adding a fourth (finer) lattice spacing. We note that the difference between the two results is about half standard deviation.

The outline of the paper is as follows. Section 2 contains a brief description of the $\Delta S = 2$ matrix elements of the effective weak Hamiltonian describing the most general pattern of $K^0 - \bar{K}^0$ oscillations. In section 3, based on the results of this work for the $\Delta S = 2$ B-parameters, we discuss the implications for NP of our updated Unitarity Triangle (UT) analysis [9]. In section 4 we illustrate the main theoretical features of the lattice setup employed in our simulations (twisted mass lattice QCD [10, 11]) and we describe the strategy for obtaining accurate numerical estimates of the B-parameters as well as ratios of kaon four-fermion matrix elements. In section 5 we collect our numerical results. In section 6 we give our estimates of the various B-parameters and matrix elements ratios and compare the present results with the previous determinations existing in the literature. In five appendices we discuss a number of technicalities: i) the renormalization properties of the four-fermion operators in our "mixed action" setup [12]; ii-iii) the RI-MOM computation of renormalization constants (RCs) and corresponding results respectively; iv) tables of lattice data on pseudoscalar meson masses, decay constants and bare four-fermion matrix elements; v) complete results on renormalized four-fermion matrix elements obtained by using various formulae for the chiral extrapolation and two alternative procedures for the RI-MOM determination of RCs.

---

[1]While finalizing our paper we became aware of the work of ref. [5] where B-parameters and ratios of four-fermion matrix elements have been computed at one lattice spacing with $N_f = 2+1$ dynamical quarks.

2 ΔS = 2 effective weak Hamiltonian

The general form of the $\Delta S = 2$ effective weak Hamiltonian is

$$\mathcal{H}_{\text{eff}}^{\Delta S=2} = \sum_{i=1}^{5} C_i \mathcal{O}_i + \sum_{i=1}^{3} \tilde{C}_i \tilde{\mathcal{O}}_i \,, \tag{2.1}$$

where in the so-called SUSY basis ([1, 13]) the four-fermion operators $\mathcal{O}_i$ and $\tilde{\mathcal{O}}_i$ have the form

$$\begin{aligned}
\mathcal{O}_1 &= [\bar{s}^\alpha \gamma_\mu (1 - \gamma_5) d^\alpha][\bar{s}^\beta \gamma_\mu (1 - \gamma_5) d^\beta] \\
\mathcal{O}_2 &= [\bar{s}^\alpha (1 - \gamma_5) d^\alpha][\bar{s}^\beta (1 - \gamma_5) d^\beta] \\
\mathcal{O}_3 &= [\bar{s}^\alpha (1 - \gamma_5) d^\beta][\bar{s}^\beta (1 - \gamma_5) d^\alpha] \\
\mathcal{O}_4 &= [\bar{s}^\alpha (1 - \gamma_5) d^\alpha][\bar{s}^\beta (1 + \gamma_5) d^\beta] \\
\mathcal{O}_5 &= [\bar{s}^\alpha (1 - \gamma_5) d^\beta][\bar{s}^\beta (1 + \gamma_5) d^\alpha]
\end{aligned} \tag{2.2}$$

$$\begin{aligned}
\tilde{\mathcal{O}}_1 &= [\bar{s}^\alpha \gamma_\mu (1 + \gamma_5) d^\alpha][\bar{s}^\beta \gamma_\mu (1 + \gamma_5) d^\beta] \\
\tilde{\mathcal{O}}_2 &= [\bar{s}^\alpha (1 + \gamma_5) d^\alpha][\bar{s}^\beta (1 + \gamma_5) d^\beta] \\
\tilde{\mathcal{O}}_3 &= [\bar{s}^\alpha (1 + \gamma_5) d^\beta][\bar{s}^\beta (1 + \gamma_5) d^\alpha]
\end{aligned} \tag{2.3}$$

with α and β denoting color indices. Spin indices are implicitly contracted within square brackets. The Wilson coefficients C_i and $\tilde{C}_i$ have an implicit renormalization scale dependence which is compensated by the scale dependence of the renormalization constants of the corresponding operators.

Notice that the parity-even parts of the operators $\mathcal{O}_i$ and $\tilde{\mathcal{O}}_i$ are equal. From now on and for notational simplicity we will denote by O_i ($i = 1, \ldots, 5$) the parity-even components of the operators (2.2). Due to parity conservation in strong interactions, in the study of $\bar{K}^0 - K^0$ oscillations it is then sufficient to consider only the matrix elements $\langle \bar{K}^0 | O_i | K^0 \rangle$. We recall that in the SM only the kaon matrix element of the operator $\mathcal{O}_1$ comes into play.

The bag parameters, B_i ($i = 1, \ldots, 5$), provide the value of four-fermion matrix elements in units of the magnitude of their vacuum saturation approximation. More explicitly they are defined by the equations [14]

$$\langle \bar{K}^0 | O_1(\mu) | K^0 \rangle = \xi_1 \, B_1(\mu) \, m_K^2 f_K^2 \tag{2.4}$$

$$\langle \bar{K}^0 | O_i(\mu) | K^0 \rangle = \xi_i \, B_i(\mu) \left[\frac{m_K^2 f_K}{m_s(\mu) + m_d(\mu)} \right]^2 \quad \text{for} \quad i = 2, \ldots, 5, \tag{2.5}$$

with $\xi_i = (8/3, -5/3, 1/3, 2, 2/3)$. In the above relations one recognizes B_1 as the familiar B_K. We recall that, as suggested by the parametrization adopted in the r.h.s. of eqs. (2.4) and (2.5), the $\langle \bar{K}^0 | O_1(\mu) | K^0 \rangle$ matrix element is expected to vanish in the chiral limit unlike the other four ones.

An alternative way which has the merit of allowing a more accurate evaluation of matrix elements, is to consider the matrix elements ratios $R_i = \langle \bar{K}^0 | O_i | K^0 \rangle / \langle \bar{K}^0 | O_1 | K^0 \rangle$, $i = 2, \ldots, 5$, as first proposed in ref. [6]. For details on our lattice implementation see section 4 and in particular eq. (4.19).

$\overline{\text{MS}}$ (2 GeV)				
B_1	B_2	B_3	B_4	B_5
0.53(2)	0.52(2)	0.89(5)	0.79(3)	0.61(4)
R_1	R_2	R_3	R_4	R_5
1	-14.0(5)	4.8(3)	24.3(8)	6.6(4)

Table 1. Continuum limit results for B_i and R_i, renormalized in the $\overline{\text{MS}}$ scheme of ref. [15] at 2 GeV.

RI-MOM (2 GeV)				
B_1	B_2	B_3	B_4	B_5
0.52(2)	0.70(2)	1.22(7)	1.00(4)	0.73(5)
R_1	R_2	R_3	R_4	R_5
1	-12.9(4)	4.5(2)	21.1(7)	5.3(3)

Table 2. Continuum limit results for B_i and R_i, renormalized in the RI-MOM scheme at 2 GeV.

For the reader's convenience we here anticipate our final continuum results for B_i and R_i in the $\overline{\text{MS}}$ scheme of Buras et al., defined in ref. [15], and the RI-MOM scheme[2] at 2 GeV, see tables 1 and 2 respectively. Details on the calculation and uncertainty estimates are given in section 5. In appendix E we also give the final continuum results for B_i and R_i in the $\overline{\text{MS}}$ and the RI-MOM scheme at 3 GeV.

3 Model-independent constraints on $\Delta S = 2$ operators and New Physics scale from the Unitarity Triangle analysis

$\Delta F = 2$ processes provide some of the most stringent constraints on NP generalizations of the SM. Several phenomenological analyses of $\Delta F = 2$ processes have been performed in the last years, both for specific NP models and in model-independent frameworks. A generalization of the UT analysis, which allows for NP effects by including the most significant flavour constraints on NP available at the time was performed in ref. [9]. The result was a simultaneous determination of the CKM parameters and the size of NP contributions to $\Delta F = 2$ processes in the neutral kaon and $B_{d,s}$ meson sectors.

The NP generalization of the UT analysis consists in including in the theoretical parametrization of the various observables the matrix elements of operators which, though absent in the SM, may appear in some of its extensions. The analysis shows that the constraints coming from $K^0 - \bar{K}^0$ matrix elements are the most stringent ones, in particular for models that generate transitions between quarks of different chiralities (see refs. [1]–[4]). Thus an accurate determination of the $\Delta S = 2$ B-parameters is crucial to the improvement of the NP constraints.

---

[2]Actually, instead of the standard version of the RI-MOM scheme defined in [16] we employ the RI'-MOM scheme [17]. The prime on RI is to remind about the specific definition we adopted for the quark field RC, $Z_q = \Sigma_1$, where Σ_1 is the quark propagator form factor defined in eq. (3.5) of ref. [18].

The results for the $\Delta S = 2$ B-parameters obtained in the present work come from unquenched $N_f = 2$ lattice QCD data carefully extrapolated to the continuum limit. They hence represent a significant progress with respect to the input values used in the UT analysis performed in ref. [9], where quenched lattice numbers (without a systematic continuum limit extrapolation analysis) computed more than five years ago in refs. [6] and [7] were employed. For this reason, we present here an update of the analysis of ref. [9] based on our new values of the $\Delta S = 2$ B-parameters. The new ingredients entering the analysis are collected in tables 1 and 2. For all the other input data we use the numbers quoted in ref. [19] in the Summer 2012 analysis.

In the present NP-oriented analysis, the relations among experimental observables and the CKM matrix elements are extended by taking into consideration the most general form of the $\Delta S = 2$ effective weak Hamilonian (see eq. (2.1)). The effective weak Hamilonian is parameterized by Wilson coefficients of the form

$$C_i(\Lambda) = \frac{F_i L_i}{\Lambda^2}, \qquad i = 2, \dots, 5, \tag{3.1}$$

where F_i is the (generally complex) relevant NP flavor coupling, L_i is a (loop) factor which depends on the interactions that generate $C_i(\Lambda)$, and Λ is the scale of NP, i.e. the typical mass of new particles mediating $\Delta S = 2$ transitions. For a generic strongly interacting theory with an unconstrained flavor structure, one expects $F_i \sim L_i \sim 1$, so that the phenomenologically allowed range for each of the Wilson coefficients can be immediately translated into a lower bound on Λ. Specific assumptions on the flavor structure of NP correspond to special choices of the F_i functions. For example Minimal Flavor Violation (MFV) models [20]–[25] correspond to $F_1 = F_{\rm SM}$ and $F_{i \neq 1} = 0$.

Following ref. [9], in deriving the lower bounds on the NP scale Λ, we assume $L_i = 1$, that corresponds to strongly-interacting and/or tree-level coupled NP. Two other interesting possibilities are given by loop-mediated NP contributions proportional to either α_s^2 or α_W^2. The first case corresponds for example to gluino exchange in the minimal supersymmetric SM. The second case applies to all models with SM-like loop-mediated weak interactions. To obtain the lower bound on Λ entailed by loop-mediated contributions, one simply has to multiply the bounds we quote in the following by $\alpha_s(\Lambda) \sim 0.1$ or $\alpha_W \sim 0.03$.

In agreement with ref. [9], we find that in the K^0 sector, due to the non-vanishing chiral limit (chiral enhancement) of their matrix elements, all bounds coming from the contributions of non-standard operators (i.e. from the operators O_i with $i \neq 1$) are more than one order of magnitude stronger than the bound from the SM O_1 operator.

The results for the upper bounds on the Im C_i^K coefficients and the corresponding lower bounds on the NP scale Λ are collected in table 3 where they are compared to the previous results of ref. [9]. The superscript K is to recall that we are reporting the bounds coming from the kaon sector we are here analyzing. Although several input parameters have been updated with respect to ref. [9] (see ref. [19]), the more stringent constraints on the Wilson coefficients of the non-standard operators and, consequently, on the NP scale, mainly come from the improved accuracy achieved in the values of the $\Delta S = 2$ B-parameters obtained in the present work. This can be realized by comparing the small improvement of the bound

	95% allowed range	Lower limit on Λ
	(GeV^{-2})	(TeV)
$\text{Im}\, C_1^K$	$[-2.1, 3.4] \cdot 10^{-15}$	$1.7 \cdot 10^4$
$\text{Im}\, C_2^K$	$[-2.1, 1.4] \cdot 10^{-17}$	$22 \cdot 10^4$
$\text{Im}\, C_3^K$	$[-5.1, 7.8] \cdot 10^{-17}$	$11 \cdot 10^4$
$\text{Im}\, C_4^K$	$[-3.0, 4.7] \cdot 10^{-18}$	$46 \cdot 10^4$
$\text{Im}\, C_5^K$	$[-0.9, 1.4] \cdot 10^{-17}$	$27 \cdot 10^4$
$\text{Im}\, C_1^K$	$[-4.4, 2.8] \cdot 10^{-15}$	$1.5 \cdot 10^4$
$\text{Im}\, C_2^K$	$[-5.1, 9.3] \cdot 10^{-17}$	$10 \cdot 10^4$
$\text{Im}\, C_3^K$	$[-3.1, 1.7] \cdot 10^{-16}$	$5.7 \cdot 10^4$
$\text{Im}\, C_4^K$	$[-1.8, 0.9] \cdot 10^{-17}$	$24 \cdot 10^4$
$\text{Im}\, C_5^K$	$[-5.2, 2.8] \cdot 10^{-17}$	$14 \cdot 10^4$

Table 3. 95% probability range for the $\text{Im}\, C_K^i$ coefficients and the corresponding lower bounds on the NP scale, Λ, for a generic strongly interacting NP with generic flavor structure ($L_i = F_i = 1$). In the lower panel the results of [9] are displayed for comparison.

coming from $\text{Im}\, C_1^K$, obtained using a value of the B_1-parameter very close to the one taken in ref. [9], with those coming from the other coefficients using the new B-parameters. We observe that the analysis is performed (as in [9]) by switching on one coefficient at the time in each sector, thus excluding the possibility of having accidental cancellations among the contributions of different operators. Therefore, the reader should keep in mind that the bounds may be weakened if, instead, some accidental cancellation occurs.

In figure 1 we show the comparison between the lower bounds on the NP scale obtained for the case of a generic strongly interacting NP with generic flavor structure by the constraints on the $\text{Im}\, C_i^K$ coefficients coming from the present generalized UT analysis, and the previous results of ref. [9].

As a specific example of NP models we consider the warped five-dimensional extensions of the SM discussed in ref. [26], where the origin of hierarchies in quark masses and mixings is explained via the localization properties of quark wave functions in the fifth dimension. In particular, in the Randall-Sundrum (RS) scenario one has

$$L_4 = (g_s^*)^2, \quad F_4 = \frac{2 m_d m_s}{Y_*^2 v^2}, \quad \Lambda = M_G, \tag{3.2}$$

where M_G and $g_s^* \sim 6$ are the mass and coupling of Kaluza-Klein excitations of the gluon, $Y_* \sim 3$ is the five-dimensional Yukawa coupling (whose flavour structure is assumed to be anarchic), $m_d \sim 3\,\text{MeV}$ and $m_s \sim 50\,\text{MeV}$ are $\overline{\text{MS}}$ quark masses at the high scale and $v = 246\,\text{GeV}$ is the Higgs vev. Running from a reference scale of $5\,\text{TeV}$, we obtain at 95% probability $\text{Im}\, C_4^K \in [-4.7, 10.6] \cdot 10^{-18}$, from which we get

$$M_G > 43\,\text{TeV}. \tag{3.3}$$
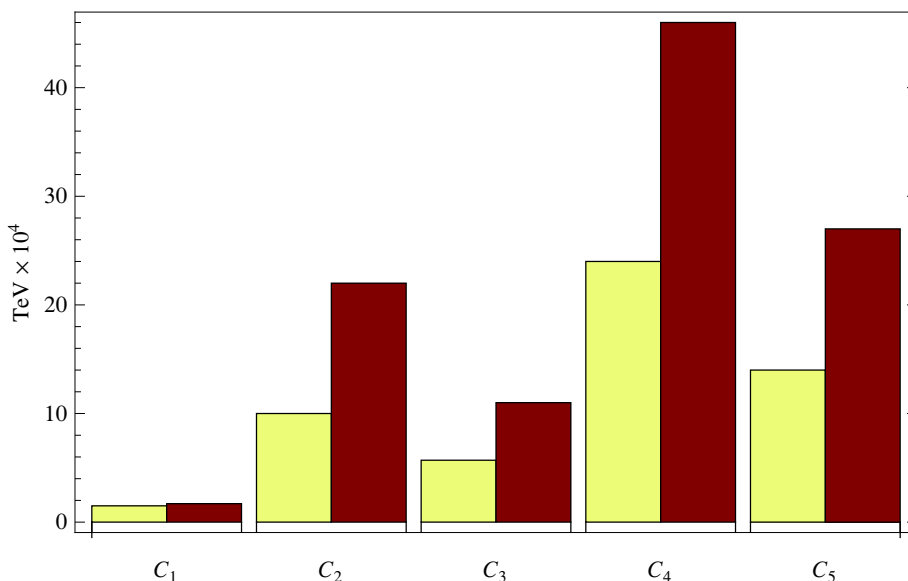
Figure 1. The lower bounds on the NP scale, provided by the constraints on $\mathrm{Im}\, C_i^K$ $(i = 1, \ldots, 5)$ for generic NP flavor structure, are shown as brown bars. For comparison, we plot the bounds of ref. [9] as yellow bars.

Considering instead gauge-Higgs unification (GHU) models, from ref. [26] we have

$$L_4 = (g_s^*)^2\,, \quad F_4 \sim \frac{8 m_d m_s}{g_*^2 v^2}\,, \quad \Lambda = M_G\,, \tag{3.4}$$

where in this case $g_* \sim 4$ is the five-dimensional gauge coupling in units of the radius of the compact dimension. We obtain the bound

$$M_G > 65\,\mathrm{TeV}. \tag{3.5}$$

4 Non-perturbative lattice computation of the $\Delta S = 2$ matrix elements

Lattice QCD provides an ideal first principle framework in which non-perturbative computation of hadronic matrix elements can be performed with controlled systematic uncertainties. In the last few years a number of lattice determinations of B_K of increasing precision have appeared in the literature based on a variety of lattice regularizations with $N_f = 2$ or $N_f = 3$ dynamical fermions [8], [27]–[31]. For recent reviews see refs. [32]–[34].

Very little has been done in the literature concerning the calculation of the physical matrix elements of the full operator basis of eq. (2.2). Calculations of the whole set of $\Delta S = 2$ renormalized operators have been carried out, in the quenched approximation, using improved Wilson fermions (see refs. [6] and [14]) or the chirality conserving overlap and domain-wall fermions (see refs. [7] and [36], respectively). Very recently a $N_f = 2 + 1$

dynamical quark calculation appeared [5] that uses domain-wall fermions at one value of the lattice spacing.[3]

The first calculation of the kaon matrix elements of the whole operator basis was performed employing Clover improved Wilson fermions. Since the Clover term coefficient was set to its tree-level value, matrix elements were affected by $O(g_0^2 a)$ discretization errors. Simulations were carried out at two values of the gauge coupling corresponding to lattice spacings ~ 0.07 and ~ 0.09 fm ([6, 14]). The major source of systematic errors was, however, the uncertainty related to the construction of the multiplicatively renormalizable lattice operators O_i. In fact, owing to the breaking of the chiral symmetry intrinsic in the Wilson fermion action, the bare counterparts of each of them mix with all the other operators of equal dimension including those with "wrong" chiral transformation properties [37]. All the mixing coefficients and the overall RC were computed in the non-perturbative RI-MOM scheme [16].

Similar quenched computations were carried out using overlap and domain-wall fermions (see refs. [7] and [36], respectively). Though performed at pretty coarse lattice spacings (namely $a \sim 0.09$ and ~ 0.13 fm in the case of overlap fermions and $a \sim 0.1$ fm in the case of domain-wall fermions), these simulations have the advantage that the renormalization properties of the operators entering the four-fermion basis are as in the continuum, and lattice artifacts are $O(a^2)$. Also in this case the non-perturbative RI-MOM scheme was used in the computation of the various RCs.

In the following sections we present a new unquenched computation of the kaon matrix elements of the full $\Delta S = 2$ four-fermion operator basis employing lattice data from simulations with $N_f = 2$ dynamical fermions, performed at four rather fine values of the lattice spacing in the interval $[0.05, 0.1]$ fm. We are thus able to safely extrapolate the lattice estimators of all the relevant matrix elements to the continuum limit (CL).

We use a mixed fermion action setup where we adopt different regularizations for sea and valence quarks. In particular we introduce maximally twisted (Mtm) sea quarks [11] that we take in combination with Osterwalder-Seiler (OS) [38] valence quarks. This strategy has been suggested in ref. [12] as a way of setting up a computational framework allowing for a calculation of $\Delta S = 2$ four-fermion matrix elements that is both automatically $O(a)$ improved and free of wrong chirality mixing effects. A proof of the latter point is given in appendix A and its validity is numerically verified in appendix B, while $O(a)$ improvement of physical quantities is a genuine property of the setup of ref. [12]. As a consequence unitarity violations due to different sea and valence quark regularization yield only $O(a^2)$ artifacts, provided renormalized sea and valence quark masses are matched. In our case, the matching of the renormalized quark masses is obtained by simply taking identical values for the corresponding sea and valence bare mass parameters.

The interesting lattice setup briefly described above has already been successfully tested in B_K computations both in the quenched approximation [39] and on ensembles with $N_f = 2$ [8] and $N_f = 2 + 1 + 1$ dynamical quarks [40], as well as in unquenched ($N_f = 2 + 1 + 1$) studies of meson masses and decay constants [41] and nucleon sigma terms [42].

---

[3]A preliminary computation of the bare matrix elements using unquenched $N_f = 2 + 1$ domain-wall dynamical fermions was presented in ref. [35].

4.1 Sea and valence quark regularization

The Mtm-LQCD action of the light quark flavor doublet can be written in the so-called "physical basis" in the form [11]

$$
S_{\text{sea}}^{\text{Mtm}} = a^4 \sum_x \bar{\psi}(x) \left\{ \frac{1}{2} \sum_\mu \gamma_\mu (\nabla_\mu + \nabla_\mu^*) - i\gamma_5 \tau^3 r_{\text{sea}} \left[M_{\text{cr}} - \frac{a}{2} \sum_\mu \nabla_\mu^* \nabla_\mu \right] + \mu_{\text{sea}} \right\} \psi(x). \quad (4.1)
$$

The subscript *sea* is to remind us that this action will be used to generate unquenched gauge configurations. The field ψ describes a mass degenerate up and down doublet with bare (twisted) mass μ_{sea}. The parameter M_{cr} is the critical mass that one has to fix non-perturbatively at its optimal value (as proposed in refs. [43]–[45] and implemented in refs. [46] and [47]) to guarantee the O(a)-improvement of physical observables and get rid of all the unwanted leading chirally enhanced cutoff effects. In the gauge sector the tree-level improved action proposed in ref. [48] has been used.

For valence quarks we use the OS regularization [38]. The full valence action is given by the sum of the contributions of each *individual* valence flavour q_f and reads [12]

$$
S_{\text{val}}^{\text{OS}} = a^4 \sum_{x,f} \bar{q}_f(x) \left\{ \frac{1}{2} \sum_\mu \gamma_\mu (\nabla_\mu + \nabla_\mu^*) - i\gamma_5 r_f \left[M_{\text{cr}} - \frac{a}{2} \sum_\mu \nabla_\mu^* \nabla_\mu \right] + \mu_f \right\} q_f(x), \quad (4.2)
$$

where the index f labels the valence flavors and M_{cr} is the same critical mass parameter which appears in eq. (4.1). We denote by r_f and μ_f the values of the Wilson parameter and the twisted quark mass of each valence flavor.

4.2 Lattice operators and correlation functions

In the strategy proposed in ref. [12], which we follow here, four species of OS valence quark flavors (q_f, $f = 1, \ldots, 4$) are introduced, two of which (q_1 and q_3) will represent the valence strange quark with masses $\mu_1 = \mu_3 \equiv \mu_{\text{``}s\text{''}}$, while the other two ($q_2$ and q_4) will be identified with the light up/down quarks having masses $\mu_2 = \mu_4 \equiv \mu_\ell$. The corresponding r_f Wilson parameters must obey the relation

$$
r_1 = r_2 = r_3 = -r_4. \quad (4.3)
$$

In the numerical computations reported in the present work we have averaged over the two cases $r_1 = \pm 1$, holding r_2, r_3 and r_4 related to r_1 as in eq. (4.3).

As in the case of the computation of $B_K (\equiv B_1)$, in the calculation of the bag parameters B_i ($i = 2, \ldots, 5$), we need to consider the axial currents

$$
A_\mu^{12} = \bar{q}_1 \gamma_\mu \gamma_5 q_2 \qquad A_\mu^{34} = \bar{q}_3 \gamma_\mu \gamma_5 q_4. \quad (4.4)
$$

and the pseudoscalar quark densities

$$
P^{12} = \bar{q}_1 \gamma_5 q_2 \qquad P^{34} = \bar{q}_3 \gamma_5 q_4. \quad (4.5)
$$

In addition, we need to consider the following set of four-fermion operators

$$O_{1[\pm]}^{MA} = 2\big\{ \big([\bar{q}_1^\alpha \gamma_\mu q_2^\alpha][\bar{q}_3^\beta \gamma_\mu q_4^\beta] + [\bar{q}_1^\alpha \gamma_\mu \gamma_5 q_2^\alpha][\bar{q}_3^\beta \gamma_\mu \gamma_5 q_4^\beta]\big) \pm (2 \leftrightarrow 4) \big\}$$

$$O_{2[\pm]}^{MA} = 2\big\{ \big([\bar{q}_1^\alpha q_2^\alpha][\bar{q}_3^\beta q_4^\beta] + [\bar{q}_1^\alpha \gamma_5 q_2^\alpha][\bar{q}_3^\beta \gamma_5 q_4^\beta]\big) \pm (2 \leftrightarrow 4) \big\}$$

$$O_{3[\pm]}^{MA} = 2\big\{ \big([\bar{q}_1^\alpha q_2^\beta][\bar{q}_3^\beta q_4^\alpha] + [\bar{q}_1^\alpha \gamma_5 q_2^\beta][\bar{q}_3^\beta \gamma_5 q_4^\alpha]\big) \pm (2 \leftrightarrow 4) \big\}$$

$$O_{4[\pm]}^{MA} = 2\big\{ \big([\bar{q}_1^\alpha q_2^\alpha][\bar{q}_3^\beta q_4^\beta] - [\bar{q}_1^\alpha \gamma_5 q_2^\alpha][\bar{q}_3^\beta \gamma_5 q_4^\beta]\big) \pm (2 \leftrightarrow 4) \big\}$$

$$O_{5[\pm]}^{MA} = 2\big\{ \big([\bar{q}_1^\alpha q_2^\beta][\bar{q}_3^\beta q_4^\alpha] - [\bar{q}_1^\alpha \gamma_5 q_2^\beta][\bar{q}_3^\beta \gamma_5 q_4^\alpha]\big) \pm (2 \leftrightarrow 4) \big\} , \qquad (4.6)$$

where square parentheses denote spin invariants and α and β are color indices.

In the mixed action (MA) approach defined above the following properties can be proved (see appendix A and ref. [12]).

(i) The operators $O_{i[+]}^{MA}$ defined in eq. (4.6) enjoy continuum-like renormalization properties,

$$\begin{pmatrix} O_{1[+]}^{MA} \\ O_{2[+]}^{MA} \\ O_{3[+]}^{MA} \\ O_{4[+]}^{MA} \\ O_{5[+]}^{MA} \end{pmatrix}_{\text{ren}} = \begin{pmatrix} Z_{11} & 0 & 0 & 0 & 0 \\ 0 & Z_{22} & Z_{23} & 0 & 0 \\ 0 & Z_{32} & Z_{33} & 0 & 0 \\ 0 & 0 & 0 & Z_{44} & Z_{45} \\ 0 & 0 & 0 & Z_{54} & Z_{55} \end{pmatrix} \begin{pmatrix} O_{1[+]}^{MA} \\ O_{2[+]}^{MA} \\ O_{3[+]}^{MA} \\ O_{4[+]}^{MA} \\ O_{5[+]}^{MA} \end{pmatrix} \qquad (4.7)$$

where the matrix Z_{ij} is defined in eqs. (A.7), (A.9) and (A.10).

(ii) The axial currents and pseudoscalar quark densities, defined in eqs. (4.4) and (4.5), are renormalized according to the formulae ([12, 18])

$$[A_\mu^{12}]_{\text{ren}} = Z_A A_\mu^{12} \qquad\qquad [A_\mu^{34}]_{\text{ren}} = Z_V A_\mu^{34} , \qquad (4.8)$$

$$[P^{12}]_{\text{ren}} = Z_S P^{12} \qquad\qquad [P^{34}]_{\text{ren}} = Z_P P^{34} . \qquad (4.9)$$

(iii) The matrix elements $\langle P^{43}|O_{i[+]}^{MA}|P^{12}\rangle_{\text{ren}}$, obtained from correlation functions of the renormalized operators in eqs. (4.7)–(4.9), with the identification $\mu_1 = \mu_3 = \mu_s$ (= bare strange quark mass) and $\mu_2 = \mu_4 = \mu_\ell$ (= bare up-down quark mass), will tend in the limit $a \to 0$ to the continuum matrix elements $\langle \bar{K}^0|O_i|K^0\rangle$ of the (parity-even parts of the) operators of eq. (2.2) with mere $\mathrm{O}(a^2)$ discretization errors.

The key statement (iii) follows by noting that the set of fermionic Wick contractions contributing to the three-point correlation functions (see eq. (4.11) below) from which the matrix elements $\langle P^{43}|O_{i[+]}^{MA}|P^{12}\rangle_{\text{ren}}$ are extracted coincides with the set of Wick contractions in the the three-point continuum QCD correlator relevant for the computation of the matrix elements $\langle \bar{K}^0|O_i|K^0\rangle$ and by exploiting the general renormalizability and $\mathrm{O}(a)$ improvement properties of our MA lattice setup (spelled out in ref. [12]), as well as the renormalization properties (4.7) of the operators $O_{i[+]}^{MA}$. Concerning the issue of $\mathrm{O}(a)$ improvement we recall here that

- the bare matrix elements of $O_{i[+]}^{MA}$'s are free from $O(a)$ cutoff effects;

- the relevant renormalization constants in the RI-MOM scheme can also be evaluated with no $O(a)$ artefacts.

The first of these properties was derived in ref. [12] for generic hadron masses and matrix elements.[4] The second property above follows from the remark that the one-particle-irreducible vertices entering the RI-MOM renormalization conditions are $O(a)$ improved in our MA setup, just because such vertices turn out to be invariant under parity transformations of their external momenta. The argument here is closely analogous to the one presented for the renormalization constants of quark bilinear operators in the appendix of ref. [18].

In the construction of correlation functions we follow the general procedure outlined in ref. [8]. We use periodic boundary conditions in every direction for all fields, except for the quark fields on which we impose anti-periodic boundary conditions in the time direction. At time slices y_0 and $y_0 + T/2$ "wall" operators with K^0-meson quantum numbers are inserted. The first operator is constructed in terms of $\bar{q}_2$ and q_1 quark fields and the second in terms of $\bar{q}_4$ and q_3 quark fields. Explicitly they have the expressions

$$\mathcal{P}_{y_0}^{21} = \left(\frac{a}{L}\right)^3 \sum_{\vec{y}} \bar{q}_2(\vec{y}, y_0)\gamma_5 q_1(\vec{y}, y_0)$$

$$\mathcal{P}_{y_0+\frac{T}{2}}^{43} = \left(\frac{a}{L}\right)^3 \sum_{\vec{y}} \bar{q}_4(\vec{y}, y_0 + T/2)\gamma_5 q_3(\vec{y}, y_0 + T/2) \quad (4.10)$$

The correlators we then need to compute are[5]

$$C_i(x_0) = \left(\frac{a}{L}\right)^3 \sum_{\vec{x}} \langle \mathcal{P}_{y_0+\frac{T}{2}}^{43} O_{i[+]}^{MA}(\vec{x}, x_0) \mathcal{P}_{y_0}^{21} \rangle, \quad i = 1, \ldots, 5, \quad (4.11)$$

$$C_{PP}(x_0) = \left(\frac{a}{L}\right)^3 \sum_{\vec{x}} \langle P^{12}(\vec{x}, x_0) \mathcal{P}_{y_0}^{21} \rangle, \quad (4.12)$$

$$C_{PP}'(x_0) = \left(\frac{a}{L}\right)^3 \sum_{\vec{x}} \langle \mathcal{P}_{y_0+\frac{T}{2}}^{43} P^{34}(\vec{x}, x_0) \rangle. \quad (4.13)$$

To improve the signal-to-noise ratio a sum has been performed over the spatial position of the four-fermion operator, and for each gauge configuration the time slice y_0 is randomly chosen. An important contribution to the reduction of statistical fluctuations comes also from summing over the spatial position of both kaon interpolating fields in eq. (4.11). After summing over the the spatial position of the four-fermion operator, which is known from experience to be crucial for the signal, to project on zero 3-momentum states, just one

---

[4]A simpler derivation might also be given along the lines of appendix A of ref. [43] exploiting the symmetries of the MA lattice setup of ref. [12].

[5]For the special case of $i = 1$, the evaluation of $B_1 = B_K$ (see ref. [8]) requires the use of the two-point correlation functions that involve the axial current and have the form $C_{A_0 P}(x_0) = \left(a/L\right)^3 \sum_{\vec{x}} \langle A_0^{12}(\vec{x}, x_0) \mathcal{P}_{y_0}^{21} \rangle$ and $C_{PA_0}'(x_0) = \left(a/L\right)^3 \sum_{\vec{x}} \langle \mathcal{P}_{y_0+\frac{T}{2}}^{43} A_0^{34}(\vec{x}, x_0) \rangle$.

further spatial sum is needed. The second spatial sum, which we are able to do, gives a further signal improvement. These spatial sums were implemented and carried out at a reasonably low computational price by means of the stochastic technique discussed in section 2.2 of ref. [8].

For large time separation $y_0 \ll x_0 \ll y_0 + T/2$ the (plateau of the) following ratio estimate

$$E[B_i^{(b)}](x_0) = \frac{C_i(x_0)}{C_{PP}(x_0)\, C'_{PP}(x_0)}, \quad i = 2, \ldots, 5 \tag{4.14}$$

provides an estimate of the $B_i^{(b)}$ ($i = 2, \ldots, 5$) bag parameter[6] since

$$E[B_i^{(b)}](x_0) \xrightarrow{y_0 \ll x_0 \ll y_0 + T/2} \left. \frac{\langle \bar{K}^0 | O_{i[+]}^{MA} | K^0 \rangle}{\langle \bar{K}^0 | P^{12} | 0 \rangle \langle 0 | P^{34} | K^0 \rangle} \right|^{(b)} = \xi_i\, B_i^{(b)}, \quad i = 2, \ldots, 5\,, \tag{4.15}$$

with $(\xi_2,\, \xi_3,\, \xi_4,\, \xi_5) = (-5/3,\, 1/3,\, 2,\, 2/3)$.
We also compute the ratios

$$E[R_i^{(b)}](x_0) = \frac{C_i(x_0)}{C_1(x_0)}, \qquad i = 2, \ldots, 5\,, \tag{4.16}$$

which for large time separations yield the ratios of the corresponding kaon four-fermion matrix elements, according to the formula

$$E[R_i^{(b)}](x_0) \xrightarrow{y_0 \ll x_0 \ll y_0 + T/2} \left. \frac{\langle \bar{K}^0 | O_{i[+]}^{MA} | K^0 \rangle}{\langle \bar{K}^0 | O_{1[+]}^{MA} | K^0 \rangle} \right|^{(b)} = R_i^{(b)}, \qquad i = 2, \ldots, 5\,. \tag{4.17}$$

4.3 Estimates of renormalized quantities

Recalling eqs. (4.7) and (4.9), the renormalized values of the bag parameters will be given by the formula

$$B_i = \frac{Z_{ij}}{Z_S\, Z_P}\, B_j^{(b)}, \quad i, j = 2, \ldots, 5\,. \tag{4.18}$$

where a sum over the repeated index j is understood. As for the renormalized expression of the four-fermion operator ratios of eq. (4.17), we choose to evaluate the rescaled quantity

$$\tilde{R}_i = \left(\frac{f_K}{m_K}\right)^2_{\text{expt.}} \left[\frac{M^{12}M^{34}}{F^{12}F^{34}} \frac{Z_{ij}}{Z_{11}}\, R_j^{(b)}\right]_{\text{Lat.}}, \quad i, j = 2, \ldots, 5\,, \tag{4.19}$$

where M^{lk} and F^{lk} are the mass and decay constant of the pseudoscalar meson made of the ($\bar{q}_l\, q_k$) quark pair. In order to compensate the chiral vanishing of the $\langle \bar{K}^0 | O_1 | K^0 \rangle$ matrix element we have multiplied the ratios $R_i^{(b)}$ by the factor $M^{12}M^{34}/F^{12}F^{34}$; its form has been chosen in such a way to partially compensate the lattice artifacts affecting the different lattice discretizations of kaon mesons (resulting from different choices of the OS r_f-parameters) we use. Furthermore, we have remultiplied the quantity in the square bracket by the ratio of the experimental values of the kaon decay constant ($f_K^{\text{exp}} = 156.1\,\text{MeV}$) and its mass ($m_K^{\text{exp}} = 494.4\,\text{MeV}$). The definition we get in this way is in line with the

---

[6]In the following the superscript (b) denotes bare quantities.

one proposed in ref. [7]. Based on the discussion of section 4.2 (in particular item iii), we note that in the continuum limit and at the physical values of the u/d and s quark masses the quantity $\tilde{R}_i$ of eq. (4.19) provides the right estimate for the ratio of the renormalized matrix elements of interest, i.e.

$$R_i = \frac{\langle \bar{K}^0 | O_i | K^0 \rangle}{\langle \bar{K}^0 | O_1 | K^0 \rangle} \tag{4.20}$$

We end this section by recalling that in the twisted mass mixed action setup of ref. [12] we are using, lattice estimators of physical quantities are only affected by $O(a^2)$ lattice artifacts. This is true in particular for the kaon mass and decay constant as well as for the kaon four-fermion matrix elements.

5 Simulations, data analysis and results

The ETM Collaboration has generated $N_f = 2$ configuration ensembles at four values of the inverse bare gauge coupling, β and at a number of light quark masses, μ_{sea}. The values of the simulated lattice spacings lie in the interval $[0.05, 0.1]\,\text{fm}$. Bare quark mass parameters are chosen so as to have light pseudoscalar mesons ("pions") in the range $280 \leq m_{\text{PS}} \leq 500\,\text{MeV}$ and heavy-light pseudoscalar mesons ("kaons") in the range $450 \leq m_{PS} \leq 650\,\text{MeV}$. Simulation details are given in table 4.

The value of the light u/d quark mass parameter, $a\mu_\ell$, is common to sea and valence quarks, while the heavier quark (the would-be strange quark that we denote by "s", see table 4) is quenched. As discussed in section 5.2, we will get to the physical kaon mass by suitably interpolating (extrapolating) data in $\mu_{"s"}$ (μ_ℓ) to the "physical" value μ_s ($\mu_{u/d}$), while simultaneously taking the continuum limit. The "physical" values $\mu_{u/d}$ and μ_s of the quark masses are known and can be found in ref. [49]. The quark bilinear RCs, Z_P and Z_S, have been computed in the non-perturbative RI-MOM scheme in ref. [18]. A RC computation for the full basis of the four-fermion operators using RI-MOM techniques is presented in appendix B. In appendix C we collect the values of the four-fermion RCs that are used in this work, as well as Z_P and Z_S.

5.1 Extracting bare estimates from lattice data

Bare results for the ratio of the four-fermion matrix elements $R_i^{(b)}$ (cf. eq. (4.17)) with $i = 2, \ldots, 5$ at the four β values and combinations of quark masses are listed in tables 13–16 of appendix D. In tables 17–20 of the same appendix we collect the results for the bare quantities $\xi_i B_i^{(b)}$ ($i = 2, \ldots, 5$) at each value of β.

For illustration in figure 2 we display some examples of the $B_i^{(b)}$ plateau quality at $\beta = 3.8$, 3.9, 4.05 and 4.20. Vertical dotted lines indicate the plateau region where the K^0- and the $\bar{K}^0$-state dominate the three-point correlators. Similar examples of the plateau quality for the case of the four-fermion operator ratios are illustrated in figure 3. Both figures 2 and 3 display very good signals.

$\beta = 3.80$, $a \sim 0.10\,\mathrm{fm}$			
$a\mu_\ell = a\mu_{\mathrm{sea}}$	$a^{-4}(L^3 \times T)$	$a\mu_{\text{``}s\text{''}}$	N_{stat}
0.0080	$24^3 \times 48$	0.0165, 0.0200, 0.0250	170
0.0110	`"`	`"`	180
$\beta = 3.90$, $a \sim 0.09\,\mathrm{fm}$			
0.0040	$24^3 \times 48$	0.0150, 0.0220, 0.0270	400
0.0064	`"`	`"`	200
0.0085	`"`	`"`	200
0.0100	`"`	`"`	160
0.0030	$32^3 \times 64$	`"`	300
0.0040	`"`	`"`	160
$\beta = 4.05$, $a \sim 0.07\,\mathrm{fm}$			
0.0030	$32^3 \times 64$	0.0120, 0.0150, 0.0180	190
0.0060	`"`	`"`	150
0.0080	`"`	`"`	220
$\beta = 4.20$, $a \sim 0.05\,\mathrm{fm}$			
0.0020	$48^3 \times 96$	0.016, 0.0129, 0.0142	96
0.0065	$32^3 \times 64$	`"`	144

Table 4. Details of simulation runs at $\beta =$3.80, 3.90, 4.05 and 4.20.

5.2 Computation at the physical point

Extracting physical quantities from lattice data requires performing extrapolations and/or interpolations of renormalized lattice estimators to the physical point (continuum limit and "physical" value of quark masses).

5.2.1 RCs computation and combined continuum-chiral extrapolation

We have computed the full matrix of the four-fermion operator RCs in a mass independent scheme. We carry out the non-perturbative calculation adopting the RI-MOM approach. The implementation of the RI-MOM setup has been presented in refs. [8] and [18]. We should mention that in our RC estimators cutoff effects, though parametrically of O(a^2), are numerically reduced owing to the subtraction of perturbatively evaluated O(a^2g^2) contributions. After that, two different, but by now standard [18], procedures are employed to deal with O(a^2p^2) discretization effects. The first, called M1, consists in linearly extrapolating to zero the residual (after the perturbative subtraction) O(a^2p^2) terms. The second one (so-called p^2-window method, or M2 for short) leads to RC estimates obtained by averaging data over a fixed (in physical units) and very narrow momentum interval.

We carry out continuum and chiral extrapolations in a combined way. For all bag parameters, B_i, and ratios, $\tilde{R}_i$ (see eq. (4.19)), we have tried out a fit ansatz of the following
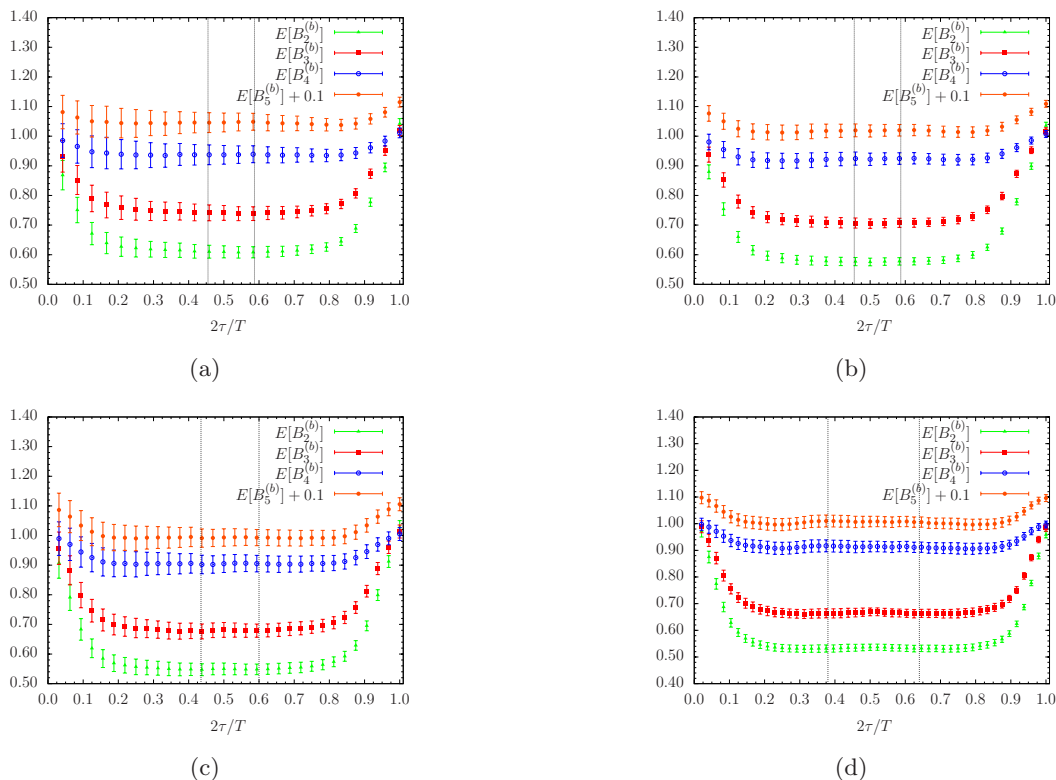
Figure 2. Data and time-plateaux for $E[B_i^{(b)}](\tau)$ $(i = 2, \ldots, 5)$ (see eq. (4.14)) plotted vs. $2\tau/T \equiv 2(x_0 - y_0)/T$. In panel (a) we show data for $\beta = 3.80$ and $(a\mu_\ell, a\mu_{\text{``}s\text{''}}) = (0.0080, 0.0165)$ on a $24^3 \times 48$ lattice; in panel (b) for $\beta = 3.90$, $(a\mu_\ell, a\mu_{\text{``}s\text{''}}) = (0.0040, 0.0150)$ on a $24^3 \times 48$ lattice; in panel (c) for $\beta = 4.05$ and $(a\mu_\ell, a\mu_{\text{``}s\text{''}}) = (0.0030, 0.0120)$ on a $32^3 \times 64$ lattice; in panel (d) for $\beta = 4.20$ and $(a\mu_\ell, a\mu_{\text{``}s\text{''}}) = (0.0020, 0.0129)$ on a $48^3 \times 96$ lattice. Vertical dotted lines delimit the plateau region. For clarity data for $E[B_5^{(b)}](\tau)$ have been slightly shifted.

general form

$$Y = \sum_{n=0}^{2} A_Y^{(n)}(r_0\hat{\mu}_s) \left[r_0 \, \hat{\mu}_\ell\right]^n + D_Y(r_0\hat{\mu}_s) \left[\frac{a}{r_0}\right]^2 , \qquad (5.1)$$

where we have made explicit the dependence of the fit parameters $A_Y^{(n)}$ and D_Y on the renormalized strange quark mass[7] in units of r_0 $(r_0\hat{\mu}_s)$. We studied separately the cases of linear and polynomial ansatz. We have also considered NLO ChPT fit functions for B_i based on the formulae given in [50] in the case of SU(3). Those formulae transformed to NLO SU(2) ChPT read:

$$B_i = B_i^\chi(r_0\hat{\mu}_s) \left[1 + b_i(r_0\hat{\mu}_s) \mp \frac{2\hat{B}_0\hat{\mu}_\ell}{2(4\pi f_0)^2} \log \frac{2\hat{B}_0\hat{\mu}_\ell}{(4\pi f_0)^2}\right] + D'_{Bi}(r_0\hat{\mu}_s) \left[\frac{a}{r_0}\right]^2 \qquad (5.2)$$

with $\hat{B}_0 = 2.84(11)\,\text{GeV}$ (renormalized in $\overline{\text{MS}}$ at $2\,\text{GeV}$) and $f_0 = 121.0(1)\,\text{MeV}$, as we used in [8]. The sign before the logarithmic term is minus (-) for $i = 1, 2, 3$ and plus (+)

---

[7]We use the symbol (ˆ) to denote renormalized quark masses in the $\overline{\text{MS}}$ scheme at $2\,\text{GeV}$.
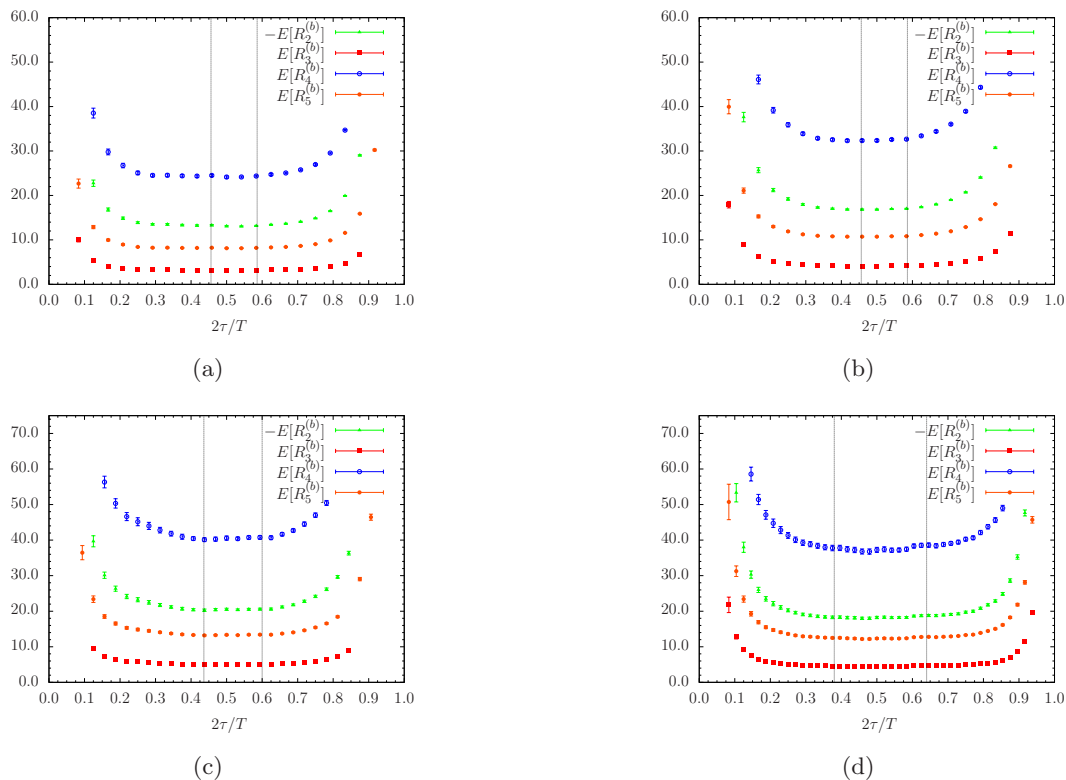
Figure 3. Data and time-plateaux for $E[R_i^{(b)}](\tau)$ $(i = 2, \ldots, 5)$ (see eq. (4.16)) plotted vs. $2\tau/T \equiv 2(x_0 - y_0)/T$. In panel (a) we show data for $\beta = 3.80$ and $(a\mu_\ell, a\mu_{\text{``}s\text{''}}) = (0.0080, 0.0165)$ on a $24^3 \times 48$ lattice; in panel (b) for $\beta = 3.90$, $(a\mu_\ell, a\mu_{\text{``}s\text{''}}) = (0.0040, 0.0150)$ on a $24^3 \times 48$ lattice; in panel (c) for $\beta = 4.05$ and $(a\mu_\ell, a\mu_{\text{``}s\text{''}}) = (0.0030, 0.0120)$ on a $32^3 \times 64$ lattice; in panel (d) for $\beta = 4.20$ and $(a\mu_\ell, a\mu_{\text{``}s\text{''}}) = (0.0020, 0.0129)$ on a $48^3 \times 96$ lattice. Vertical dotted lines delimit the plateau region.

for $i = 4, 5$. As for $\tilde{R}_i$ and $i = 2, 3$ the ChPT fit formula at NLO coincides with the linear fit ansatz, while for the cases $i = 4, 5$ we use

$$\tilde{R}_i = \tilde{R}_i^\chi(r_0\hat{\mu}_s)\left[1 + c_i(r_0\hat{\mu}_s) + \frac{2\hat{B}_0\hat{\mu}_\ell}{(4\pi f_0)^2}\log\frac{2\hat{B}_0\hat{\mu}_\ell}{(4\pi f_0)^2}\right] + D'_{Ri}(r_0\hat{\mu}_s)\left[\frac{a}{r_0}\right]^2 \qquad (5.3)$$

The (r_0/a) values are

$$\left.\frac{r_0}{a}\right|_\beta = \{4.54(7), \ 5.35(4), \ 6.71(4), \ 8.36(6)\} \qquad (5.4)$$

at $\beta = \{3.80, 3.90, 4.05, 4.20\}$ respectively.

The u/d and s quark masses have been computed in ref. [49]. Their values in the $\overline{\text{MS}}$ scheme at $2\,\text{GeV}$ are

$$\mu_{u/d}^{\overline{\text{MS}}}(2\,\text{GeV}) = 3.6(2) \ \text{MeV}, \qquad \mu_s^{\overline{\text{MS}}}(2\,\text{GeV}) = 95(6) \ \text{MeV} \qquad (5.5)$$

In the four panels of figure 4 we show the combined chiral and continuum fit (see eq. (5.1) and eq. (5.3)) for the ratios $\tilde{R}_i$ against the renormalized light quark mass for
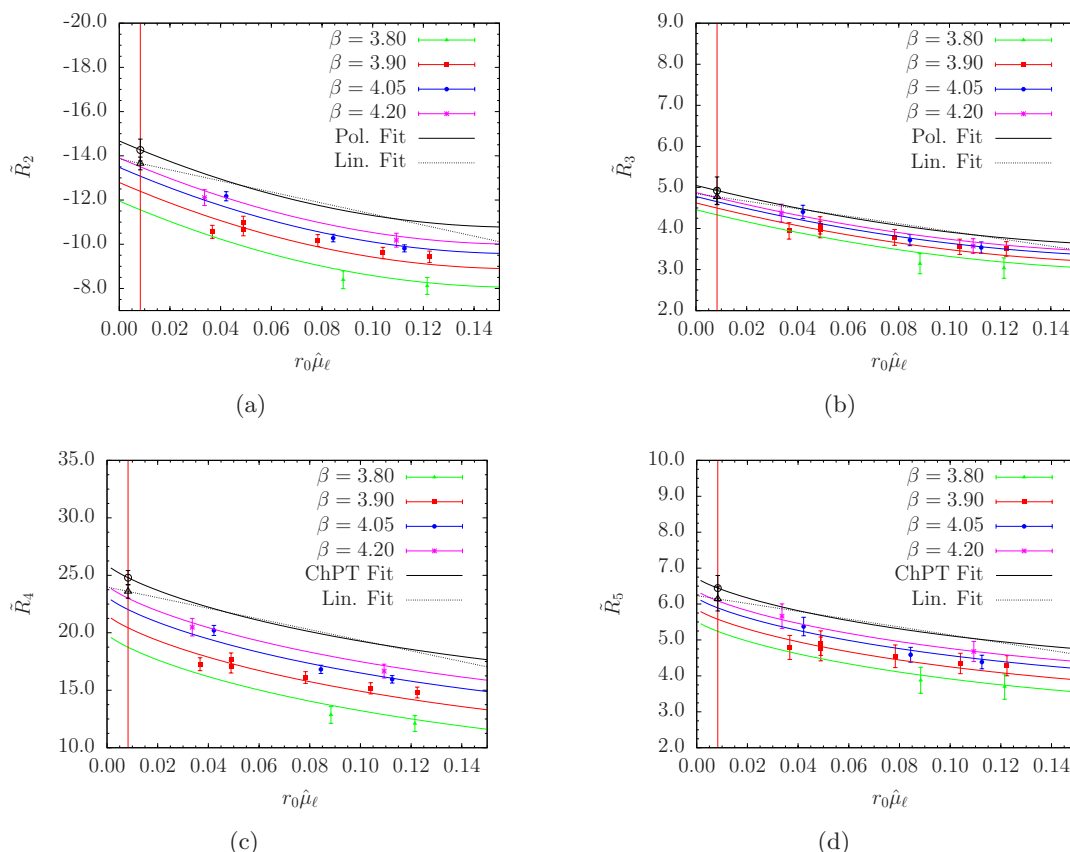
Figure 4. Solid lines in panels (a) and (b) show the behaviour vs. the renormalized light quark mass of the combined chiral and continuum fits (according to the polynomial formula (5.1) with $n = 2$) of the $\tilde{R}_i$ ratios, with $i = 2$ and $i = 3$ respectively, renormalized in the $\overline{\text{MS}}$ scheme of ref. [15] at $2\,\text{GeV}$ with the M1-type RCs. The full black line is the continuum limit curve. In panels (c) and (d), solid lines, instead, show the combined chiral and continuum fit described by NLO-ChPT, eq. (5.3) for $i = 4$ and $i = 5$, respectively. The full black line is the continuum limit curve. The dashed black line represents the continuum limit curve in the case of the linear fit ansatz. Black open circles and triangles stand for the results at the physical point corresponding to the polynomial (panels (a) and (b)) and ChPT fit (panels (c) and (d)), and linear fit ansatz, respectively.

$i = 2, \ldots, 5$, respectively. The RCs used in these plots are the ones computed with the M1-method and are expressed in the $\overline{\text{MS}}$ scheme of ref. [15] at $2\,\text{GeV}$. Lattice data correspond to points taken at the pair of quark masses $(r_0\hat{\mu}_\ell, r_0\hat{\mu}_s)$.

In panels (a) and (b) (corresponding to cases with $i = 2, 3$ respectively) we display the curves that correspond to the polynomial fit function (5.1) at the four β values we are considering in this paper. The black solid line represents the continuum limit curve. The dashed black line represents the continuum limit curve that is obtained if a linear fit ansatz in $\hat{\mu}_\ell$ is used. Black open circles and triangles stand for the results at the physical quark mass point from the polynomial and the linear fit ansatz, respectively. Recall that for $\tilde{R}_i$ with $i = 2, 3$ ChPT fit formula at NLO coincides with a linear fit ansatz. In panels (c) and (d) (corresponding to cases with $i = 4, 5$ respectively) we display the curves corresponding to the ChPT fit formula and the linear fit function. In this case black open circles and
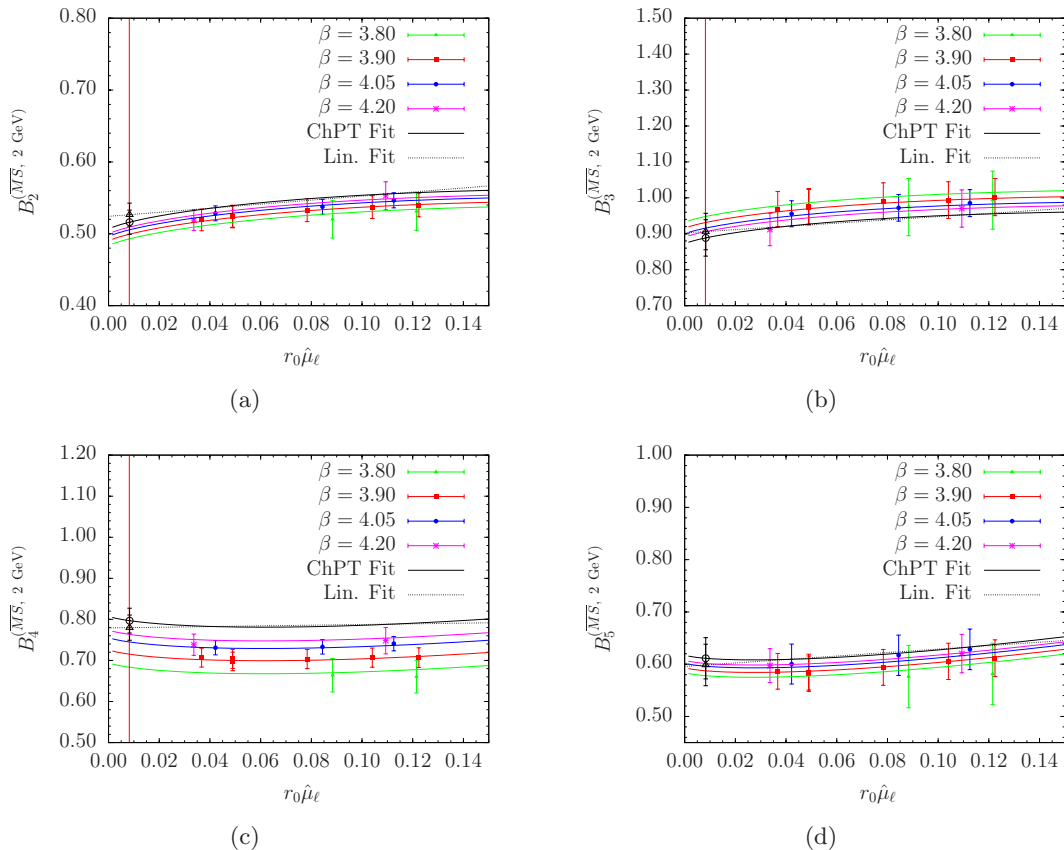
Figure 5. Solid lines in panels (a) to (d) show the behaviour vs. the renormalized light quark mass of the combined chiral and continuum fits (according to the ChPT fit formula (5.2)) for the B_i parameters with $i = 2, \ldots, 5$ respectively, renormalized in the $\overline{\text{MS}}$ scheme of ref. [15] at 2 GeV with the M1-type RCs. The full black line is the continuum limit curve (5.1). The dashed black line represents the continuum limit curve in the case of the linear fit ansatz. Black open circles and triangles stand for the results at the physical point corresponding to the ChPT fit and linear fit ansatz, respectively.

triangles stand for the results at the physical quark mass point from the ChPT fit and the linear fit ansatz, respectively.

Similarly, in figure 5 we present the combined chiral and continuum fit for the B_i-parameters, again renormalized in the $\overline{\text{MS}}$ scheme of ref. [15] at 2 GeV. In all four panels we display the curves corresponding to the ChPT fit formula at the four β values. The black solid line represents the continuum limit curve. The dashed black line represents the continuum limit curve that is obtained if a linear fit ansatz in $\hat{\mu}_\ell$ is used.

Note the nice agreement (within one standard deviation) of the two fit ansätze for both the $\tilde{R}_i$ ratios and the B_i parameters.

In tables 1 and 2 of section 2 we have gathered our final continuum results for R_i and B_i in the $\overline{\text{MS}}$ of ref. [15] and RI-MOM scheme at 2 GeV respectively. The final value of B_i for $i = 2, \ldots, 5$ has been computed by averaging the estimates obtained from the three kinds of fit ansatz discussed above, and using bootstrap error analysis. The half difference between

the two more distant results has been taken as an estimate of the systematic error associated to the extrapolation procedure. The total uncertainty is obtained by adding in quadrature the statistical and the systematic error. For $i = 1$ we update the result for B_K published in ref. [8]; note that the difference between the two results is about half standard deviation.

In appendix E we provide more detailed results obtained from the various fitting procedure we have investigated. We also show that the continuum extrapolated quantities that are eventually obtained by employing M1-type and M2-type RCs turn out to be perfectly consistent between each other within statistical errors, except for one case where cut-off effects on M2-RCs are too big for a significant comparison. Also in appendix E, see tables 23 and 24, we quote our continuum results for B_i and R_i in the $\overline{\text{MS}}$ and the RI-MOM scheme respectively at 3 GeV.

As already stated, an alternative (indirect) way to compute the ratio of the kaon matrix elements of the renormalized operators O_i, $i = 2, \ldots, 5$ to that of O_1 is based on the formula (see eqs. (2.4) and (2.5))

$$\frac{\langle \bar{K}^0 | O_i(\mu) | K^0 \rangle}{\langle \bar{K}^0 | O_1(\mu) | K^0 \rangle} = \frac{\xi_i B_i(\mu)}{\xi_1 B_1(\mu)} \frac{m_K^2}{(\hat{\mu}_s(\mu) + \hat{\mu}_d(\mu))^2} \, . \tag{5.6}$$

This of course requires knowledge of the B_i parameters and the renormalized quark masses.

We find that the two evaluations (indirect and direct, based on eq. (5.6) and eq. (4.19), respectively) lead to compatible results within errors. However, the indirect estimates suffer from much larger final uncertainties. This is due to several reasons. One is related to the quadratic dependence on the quark mass, which makes the relative error on the mass to give a significant contribution to the final error. Furthermore in the indirect method one has to consider extra uncertainties due to the error of the bilinear operators' RCs that are used to compute the B-parameters. A comparison of the direct and indirect results obtained for the ratios R_i is provided in appendix E.

6 Conclusions

Accurate measurements of the $K^0 - \bar{K}^0$ mixing amplitudes can yield useful hints on New Physics if theory can provide comparatively accurate calculations of quantities parametrizing beyond the SM effects. This requires a precise, first principle, evaluation of the kaon matrix elements of the full basis of four-fermion operators entering the most general effective $\Delta S = 2$ weak Hamiltonian.

In this paper we have presented the first unquenched lattice QCD determination in the continuum limit of the matrix elements of the full $\Delta S = 2$ four-fermion operator basis. We have used $N_f = 2$ unquenched tm-LQCD gauge configurations produced by the ETM Collaboration in combination with maximally twisted valence quarks of the OS type.

The mixed action setup proposed in ref. [12] offers the possibility of obtaining automatically O(a) improved results and an operator renormalization pattern identical to that of a chirally invariant regularization at the rather cheap price of mere O(a^2) unitarity violations. Using data at four lattice spacings (with a in the interval [0.05, 0.1] fm) and a number of pseudoscalar masses ("pions") in the range [280, 500] MeV, we are able to safely

B_i (RI-MOM at $2\,\mathrm{GeV}$)					
	This work	Ref. [7]		Ref. [6]	
	CL	$a = 0.09\,\mathrm{fm}$	$a = 0.13\,\mathrm{fm}$	$a = 0.07\,\mathrm{fm}$	$a = 0.09\,\mathrm{fm}$
1	0.52(2)	0.56(5)	0.53(4)	0.68(21)	0.70(15)
2	0.70(2)	0.87(7)	0.90(10)	0.67(7)	0.72(9)
3	1.22(7)	1.41(12)	1.53(40)	0.95(15)	1.21(10)
4	1.00(4)	0.94(5)	0.90(13)	1.00(9)	1.15(5)
5	0.73(5)	0.62(5)	0.56(14)	0.66(11)	0.88(6)

Table 5. Comparison between the unquenched results for B_i obtained in the present work and the quenched values of refs. [7] and [6]. Numbers are for renormalized quantities in the RI-MOM scheme at $2\,\mathrm{GeV}$.

R_i (RI-MOM at $2\,\mathrm{GeV}$)					
	This work	Ref. [7]		Ref. [6]	
	CL	$a = 0.09\,\mathrm{fm}$	$a = 0.13\,\mathrm{fm}$	$a = 0.07\,\mathrm{fm}$	$a = 0.09\,\mathrm{fm}$
1	1	1	1	1	1
2	-12.9(4)	-16.1(3.0)	-15.8(2.9)	-6.7(1.8)	-6.6(1.1)
3	4.5(2)	5.2(9)	5.4(8)	1.9(5)	2.3(4)
4	21.1(7)	20.7(3.0)	18.8(2.8)	12.1(3.3)	12.6(2.1)
5	5.3(3)	4.6(6)	3.9(1.3)	2.6(7)	3.3(5)

Table 6. Same as in table 5 for the R_i ratios.

carry out the continuum and the light quark mass limit of the observables of interest. All results are non-perturbatively renormalized in the RI/MOM scheme.

We get in this way the most accurate estimates to date of $\Delta S = 2$ effective weak Hamiltonian matrix elements. The total error on the R_i ratios is between 4% and 6% and on the bag parameters, B_i, between 3% and 7%.

Tables 5 and 6 show a comparison between our results for R_i and B_i (in RI/MOM at $2\,\mathrm{GeV}$) and the data at fixed lattice spacings coming from the two old quenched calculations of refs. [6] and [7].[8]

For the B-parameters, one finds large differences between the central values of our results and those of refs. [6] and [7], which vary between 5% and 25% (though the errors are typically comparably large). With respect to ref. [6], the differences are even larger when the results are compared in terms of the ratios R_i, presumably due to a combined effect, in this case, of having overestimated the values for both B_1 and the strange quark mass in the computation of [6]. We emphasize that, with respect to the old quenched calculations, having performed in the present study simulations at four values of the lattice spacing and quite smaller values of the pion masses provides us with a much better control over the main sources of systematic uncertainties, besides the quenched approximation.

---

[8]In this comparison we do not include the (preliminary) quenched results at one value of the lattice spacing given in ref. [36].

Current experience suggests that the possible systematic errors related to the quenching of the strange and charm quarks, which still affect our calculation, are negligible within the present uncertainties. Forthcoming results from simulations in the continuum limit with $N_f = 2 + 1$ and $N_f = 2 + 1 + 1$ dynamical flavours will provide a check of this expectation. We should add that our continuum limit results for R_i and B_i ($i = 2, \ldots, 5$) are in the same ballpark with the numbers given at one lattice spacing in ref. [5] where $N_f = 2 + 1$ dynamical quarks are employed.

As an interesting phenomenological application of the results obtained in this paper we have carried out a new UT analysis along the lines of the work of ref. [9]. Thanks to the improved accuracy of the present determination of the $\Delta S = 2$ B-parameters, we could substantially strengthen the existing upper bounds on the Wilson coefficients of the operators of the non-standard sector of the effective weak Hamiltonian, and consequently increase the lower bound on the New Physics scale.

Acknowledgments

A Renormalization properties of $\Delta S = 2$ four-fermion operators

In this appendix we want to spell out the renormalization properties of the four-fermion operators of interest for the description of $\bar{K}^0 - K^0$ oscillations in the mixed action (MA) lattice setup of section 4. We will do this by exploiting the results of ref. [51]. In particular, we show that the operators in eq. (4.6), that we report here for the reader convenience,

$$O_{1[\pm]}^{MA} = 2\big\{ \big([\bar{q}_1^\alpha \gamma_\mu q_2^\alpha][\bar{q}_3^\beta \gamma_\mu q_4^\beta] + [\bar{q}_1^\alpha \gamma_\mu \gamma_5 q_2^\alpha][\bar{q}_3^\beta \gamma_\mu \gamma_5 q_4^\beta]\big) \pm (2 \leftrightarrow 4) \big\}$$

$$O_{2[\pm]}^{MA} = 2\big\{ \big([\bar{q}_1^\alpha q_2^\alpha][\bar{q}_3^\beta q_4^\beta] + [\bar{q}_1^\alpha \gamma_5 q_2^\alpha][\bar{q}_3^\beta \gamma_5 q_4^\beta]\big) \pm (2 \leftrightarrow 4) \big\}$$

$$O_{3[\pm]}^{MA} = 2\big\{ \big([\bar{q}_1^\alpha q_2^\beta][\bar{q}_3^\beta q_4^\alpha] + [\bar{q}_1^\alpha \gamma_5 q_2^\beta][\bar{q}_3^\beta \gamma_5 q_4^\alpha]\big) \pm (2 \leftrightarrow 4) \big\}$$

$$O_{4[\pm]}^{MA} = 2\big\{ \big([\bar{q}_1^\alpha q_2^\alpha][\bar{q}_3^\beta q_4^\beta] - [\bar{q}_1^\alpha \gamma_5 q_2^\alpha][\bar{q}_3^\beta \gamma_5 q_4^\beta]\big) \pm (2 \leftrightarrow 4) \big\}$$

$$O_{5[\pm]}^{MA} = 2\big\{ \big([\bar{q}_1^\alpha q_2^\beta][\bar{q}_3^\beta q_4^\alpha] - [\bar{q}_1^\alpha \gamma_5 q_2^\beta][\bar{q}_3^\beta \gamma_5 q_4^\alpha]\big) \pm (2 \leftrightarrow 4) \big\}, \tag{A.1}$$

exhibit the same renormalization pattern as the corresponding continuum operators. We recall that the Wilson r-parameters of valence quarks in eq. (A.1) are taken as specified in eq. (4.3). The normalization we have chosen in the definitions (A.1) is such that, when the operators $O_{i[+]}^{MA}$ are taken between the pseudoscalar operators $P^{12} = \bar{q}_1\gamma_5 q_2$ and $P^{43} = \bar{q}_4\gamma_5 q_3$, one gets the same Wick contraction multiplicities one would obtain in QCD upon evaluating the kaon matrix elements of the operators (2.2). Naturally, apart from the issue of renormalization, the physical matrix elements will be obtained (in the continuum limit) by finally setting in our MA setup $\mu_1 = \mu_3 = \mu_s$ and $\mu_2 = \mu_4 = \mu_\ell$, with μ_s (resp. μ_ℓ) corresponding to the bare strange (resp. degenerate up-down) quark mass.

A key result of ref. [51] (stated there in the quark basis that is most natural for untwisted Wilson fermions) is that the combinations that enjoy simple renormalization properties are not the operators listed in eqs. (A.1), but those that are obtained after performing a Fierz transformation on the operators $O_{3[\pm]}^{MA}$ and $O_{5[\pm]}^{MA}$. This transformation has the effect of rewriting $O_{3[\pm]}^{MA}$ and $O_{5[\pm]}^{MA}$ in terms of operators where both spin and color indices are contracted within the same pair of quarks. With the definitions

$$
\begin{aligned}
Q_{1[\pm]}^{MA} &= 2\big\{\big([\bar{q}_1\gamma_\mu q_2][\bar{q}_3\gamma_\mu q_4] + [\bar{q}_1\gamma_\mu\gamma_5 q_2][\bar{q}_3\gamma_\mu\gamma_5 q_4]\big) \pm \big(2 \leftrightarrow 4\big)\big\} \\
Q_{2[\pm]}^{MA} &= 2\big\{\big([\bar{q}_1\gamma_\mu q_2][\bar{q}_3\gamma_\mu q_4] - [\bar{q}_1\gamma_\mu\gamma_5 q_2][\bar{q}_3\gamma_\mu\gamma_5 q_4]\big) \pm \big(2 \leftrightarrow 4\big)\big\} \\
Q_{3[\pm]}^{MA} &= 2\big\{\big([\bar{q}_1 q_2][\bar{q}_3 q_4] - [\bar{q}_1\gamma_5 q_2][\bar{q}_3\gamma_5 q_4]\big) \pm \big(2 \leftrightarrow 4\big)\big\} \\
Q_{4[\pm]}^{MA} &= 2\big\{\big([\bar{q}_1 q_2][\bar{q}_3 q_4] + [\bar{q}_1\gamma_5 q_2][\bar{q}_3\gamma_5 q_4]\big) \pm \big(2 \leftrightarrow 4\big)\big\} \\
Q_{5[\pm]}^{MA} &= 2\big\{\big([\bar{q}_1\sigma_{\mu\nu} q_2][\bar{q}_3\sigma_{\mu\nu} q_4]\big) \pm \big(2 \leftrightarrow 4\big)\big\} \quad (\text{for } \mu > \nu),
\end{aligned} \tag{A.2}
$$

where $\sigma_{\mu\nu} = [\gamma_\mu, \gamma_\nu]/2$, one gets

$$
O_{i[\pm]}^{MA} = \Lambda_{ij}^{[\pm]} Q_{j[\pm]}^{MA}, \qquad
\Lambda^{[\pm]} = \begin{pmatrix}
1 & 0 & 0 & 0 & 0 \\
0 & 0 & 0 & 1 & 0 \\
0 & 0 & 0 & \mp 1/2 & \pm 1/2 \\
0 & 0 & 1 & 0 & 0 \\
0 & \mp 1/2 & 0 & 0 & 0
\end{pmatrix} \tag{A.3}
$$

In eq. (A.2) we have omitted color indices as they are always contracted within each square parenthesis.

In order to make direct contact with the formulae of ref. [51] we must pass from the q_f-basis, in which the valence quark action (4.2) was written and where the Wilson term is (maximally) twisted, to the χ_f-basis, where the Wilson term takes its standard form. This is achieved by the chiral transformation

$$
q_f \longrightarrow \chi_f = e^{-i\pi r_f\gamma_5/4} q_f, \qquad \bar{q}_f \longrightarrow \bar{\chi}_f = \bar{q}_f e^{-i\pi r_f\gamma_5/4}, \tag{A.4}
$$

under which

$$
\begin{aligned}
S_{\text{val}}^{\text{OS}} &\to \tilde{S}_{\text{val}}^{\text{OS}} = \\
&= a^4 \sum_{x,f} \bar{\chi}_f(x)\bigg\{\frac{1}{2}\sum_\mu \gamma_\mu(\nabla_\mu + \nabla_\mu^*) + \Big[M_{\text{cr}} - \frac{a}{2}\sum_\mu \nabla_\mu^*\nabla_\mu\Big] + i\gamma_5 r_f\mu_f\bigg\}\chi_f(x),
\end{aligned} \tag{A.5}
$$

and assuming $r_4 = \pm 1$ (as used in the present work),

$$r_4 Q_{1[\pm]}^{MA} \to \tilde{Q}_{1[\pm]}^{MA} = 2i\big\{ \big([\bar{\chi}_1 \gamma_\mu \chi_2][\bar{\chi}_3 \gamma_\mu \gamma_5 \chi_4] + [\bar{\chi}_1 \gamma_\mu \gamma_5 \chi_2][\bar{\chi}_3 \gamma_\mu \chi_4]\big) \pm \big(2 \leftrightarrow 4\big) \big\}$$

$$r_4 Q_{2[\pm]}^{MA} \to \tilde{Q}_{2[\mp]}^{MA} = 2i\big\{ \big([\bar{\chi}_1 \gamma_\mu \chi_2][\bar{\chi}_3 \gamma_\mu \gamma_5 \chi_4] - [\bar{\chi}_1 \gamma_\mu \gamma_5 \chi_2][\bar{\chi}_3 \gamma_\mu \chi_4]\big) \mp \big(2 \leftrightarrow 4\big) \big\}$$

$$-r_4 Q_{3[\pm]}^{MA} \to \tilde{Q}_{3[\mp]}^{MA} = 2i\big\{ \big([\bar{\chi}_1 \gamma_5 \chi_2][\bar{\chi}_3 \chi_4] - [\bar{\chi}_1 \chi_2][\bar{\chi}_3 \gamma_5 \chi_4]\big) \mp \big(2 \leftrightarrow 4\big) \big\}$$

$$-r_4 Q_{4[\pm]}^{MA} \to \tilde{Q}_{4[\pm]}^{MA} = 2i\big\{ \big([\bar{\chi}_1 \gamma_5 \chi_2][\bar{\chi}_3 \chi_4] + [\bar{\chi}_1 \chi_2][\bar{\chi}_3 \gamma_5 \chi_4]\big) \pm \big(2 \leftrightarrow 4\big) \big\}$$

$$-r_4 Q_{5[\pm]}^{MA} \to \tilde{Q}_{5[\pm]}^{MA} = 2i\big\{ \big([\bar{\chi}_1 \sigma_{\mu\nu} \chi_2][\bar{\chi}_3 \sigma_{\mu\nu} \gamma_5 \chi_4]\big) \pm \big(2 \leftrightarrow 4\big) \big\}. \tag{A.6}$$

According to ref. [51], for the renormalized operators $\tilde{Q}_i^{MA}$ one gets

$$\begin{pmatrix} \tilde{Q}_{1[\pm]}^{MA} \\ \tilde{Q}_{2[\pm]}^{MA} \\ \tilde{Q}_{3[\pm]}^{MA} \\ \tilde{Q}_{4[\pm]}^{MA} \\ \tilde{Q}_{5[\pm]}^{MA} \end{pmatrix}^{\mathrm{ren}} = \begin{pmatrix} \mathcal{Z}_{11} & 0 & 0 & 0 & 0 \\ 0 & \mathcal{Z}_{22} & \mathcal{Z}_{23} & 0 & 0 \\ 0 & \mathcal{Z}_{32} & \mathcal{Z}_{33} & 0 & 0 \\ 0 & 0 & 0 & \mathcal{Z}_{44} & \mathcal{Z}_{45} \\ 0 & 0 & 0 & \mathcal{Z}_{54} & \mathcal{Z}_{55} \end{pmatrix}^{[\pm]} \begin{pmatrix} \tilde{Q}_{1[\pm]}^{MA} \\ \tilde{Q}_{2[\pm]}^{MA} \\ \tilde{Q}_{3[\pm]}^{MA} \\ \tilde{Q}_{4[\pm]}^{MA} \\ \tilde{Q}_{5[\pm]}^{MA} \end{pmatrix}^{(b)} \tag{A.7}$$

Since at $\mu_f = 0$ the fermion action $\tilde{S}_{\mathrm{val}}^{\mathrm{OS}}$ is indistinguishable from a standard massless Wilson fermion action, in any mass independent renormalization scheme, the operators Q_i^{MA} in the l.h.s. of eqs. (A.6) enjoy the same renormalization properties of the corresponding operators $\tilde{Q}_i^{MA}$ into which they are trasformed under (A.4). The $\tilde{Q}_i^{MA}$ operators have, up to lattice artefacts, the same RCs of the corresponding operators in the standard Wilson's formulation of lattice QCD. This result could also have been proved using the somewhat more elaborated approach of ref. [12].

From eqs. (A.6)–(A.7) and recalling eq. (A.3), one finally arrives for the operators $O_{i[+]}^{MA}$ of interest to us in this paper at the renormalization formulae

$$O_{i[+]}^{MA}\Big|^{\mathrm{ren}} = Z_{ij} O_{j[+]}^{MA}\Big|^{(b)}, \tag{A.8}$$

$$Z = \Lambda^{[+]} Z_Q (\Lambda^{[+]})^{-1}, \tag{A.9}$$

$$Z_Q = \begin{pmatrix} \mathcal{Z}_{11}^{[+]} & 0 & 0 & 0 & 0 \\ 0 & \mathcal{Z}_{22}^{[-]} & -\mathcal{Z}_{23}^{[-]} & 0 & 0 \\ 0 & -\mathcal{Z}_{32}^{[-]} & \mathcal{Z}_{33}^{[-]} & 0 & 0 \\ 0 & 0 & 0 & \mathcal{Z}_{44}^{[+]} & \mathcal{Z}_{45}^{[+]} \\ 0 & 0 & 0 & \mathcal{Z}_{54}^{[+]} & \mathcal{Z}_{55}^{[+]} \end{pmatrix} \tag{A.10}$$

From the renormalizability of (correlation functions evaluated in) the MA lattice setup of section 4 and the exact conservation of the individual valence flavours it immediately follows that the operator renormalization pattern of eqs. (A.8)–(A.10) is independent (up to cutoff effects, as usual) from the values of sea and valence quark masses. It is hence possible to determine the relevant renormalization constants in any mass-indipendent renormalization scheme by extrapolating to the chiral limit suitable renormalization constant estimators evaluated at non-vanishing quark masses. Following this strategy we computed

non-perturbatively in the RI-MOM scheme the renormalization matrix Z_Q, see eq. (A.10), as detailed in appendix B and summarized in appendix C.

At this point the matrix elements $\langle P^{43}|O_{i[+]}^{MA}|^{\text{ren}}|P^{12}\rangle|_{\text{ren}}$, built using eqs. (A.1), (A.8) and (A.10) and evaluated in our MA setup with $\mu_1 = \mu_3 = \mu_s$ (strange quark mass) and $\mu_2 = \mu_4 = \mu_\ell$ (up-down quark mass), tend in the limit $a \to 0$ to the matrix elements $\langle \bar{K}^0|O_i|K^0\rangle$ of the operators (2.2) in QCD with mere $\text{O}(a^2)$ discretization errors [12].

B RI/MOM computation of renormalization constants of four-fermion operators

In order to convert our lattice results for the bag parameters B_i to their physical continuum counterparts, in the same renormalization scheme and at the same scale as the corresponding perturbative Wilson coefficients used in the phenomenological analysis, we need the renormalization constants (RCs) of the operators $O_{i[+]}^{MA}$, $i = 1, 2, \ldots, 5$, see eq. (4.6), or equivalently eq. (A.1). As discussed in section 4, in our mixed action (MA) setup for lattice correlation functions these operators represent the analogs of the parity-even parts of the $\Delta S = 2$ four-fermion operators (2.2) that are relevant in the formal continuum theory.

In this appendix, we give details on the non-perturbative computation of the RCs performed using the RI'-MOM scheme ([17, 18]).

As explained in detail in ref. [51], instead of using the operator basis $O_{i[+]}^{MA}$ of eq. (A.1), it is more convenient to employ the Fierz transformed operators $Q_{i[+]}^{MA}$, $i = 1, 2, \ldots, 5$, defined in eq. (A.2). To lighten our notation, in the following we will drop the superscript and the sign subscript, denote these operators simply by Q_i and assemble them in the array $\mathbf{Q}$. The generic renormalization pattern of the bare operators $\mathbf{Q}^{(b)}$ is of the form

$$\mathbf{Q}^{\text{ren}} = \mathbf{Z}\,[\mathbf{I} + \boldsymbol{\Delta}]\,\mathbf{Q}^{(b)} \tag{B.1}$$

where the scale-dependent renormalization matrix $\mathbf{Z}$ is block-diagonal, with a continuum-like block structure (the same as for e.g. the matrix in eq. (A.7)), while $\boldsymbol{\Delta}$ is a sparse off-diagonal and scale-independent matrix of the form

$$\boldsymbol{\Delta} = \begin{bmatrix} 0 & \Delta_{12} & \Delta_{13} & \Delta_{14} & \Delta_{15} \\ \Delta_{21} & 0 & 0 & \Delta_{24} & \Delta_{25} \\ \Delta_{31} & 0 & 0 & \Delta_{34} & \Delta_{35} \\ \Delta_{41} & \Delta_{42} & \Delta_{43} & 0 & 0 \\ \Delta_{51} & \Delta_{52} & \Delta_{53} & 0 & 0 \end{bmatrix}. \tag{B.2}$$

However, as shown in appendix A, using the MA lattice setup of section 4, the "wrong chirality mixing" terms Δ_{ij}, are reduced to mere $\text{O}(a^2)$ effects, the renormalization matrix $\mathbf{Z}$ coincides with the matrix Z_Q of eq. (A.10) and we recover a continuum-like renormalization pattern. This is a very important advantage of our approach, which we will implement in practice using the following strategy: compute the quark propagators in the q_f-basis (also called physical basis of tmQCD at maximal twist, in which the critical Wilson term is twisted, see eq. (4.2)), impose RI-MOM renormalization conditions on the operators Q_i and extract the renormalization matrix ($\mathbf{Z}$) and, for check purposes, the mixing matrix ($\boldsymbol{\Delta}$).

B.1 Procedure for extracting the RCs

To determine the matrices $\mathbf{Z}$ and $\boldsymbol{\Delta}$ in eq. (B.1) we proceed as follows. We start by computing the lattice quark propagator

$$S_{q_f}(p) = a^4 \sum_x e^{-ipx} \langle q_f(x) \bar{q}_f(0) \rangle \tag{B.3}$$

and the four-point Green functions with an insertion of the operator Q_i, namely

$$G_i(p, p, p, p)^{a\,b\,c\,d}_{\alpha\,\beta\,\gamma\,\delta} = \tag{B.4}$$
$$a^{16} \sum_{x_1,x_2,x_3,x_4} e^{-ip(x_1-x_2+x_3-x_4)} \langle\, [q_1(x_1)]^a_\alpha\, [\bar{q}_2(x_2)]^b_\beta\, Q_i(0)\, [q_3(x_3)]^c_\gamma\, [\bar{q}_4(x_4)]^d_\delta\, \rangle\,.$$

The lower(upper) case Greek (Latin) symbols denote uncontracted spin (color) indices. The corresponding amputated Green functions are given by

$$\Lambda_i(p,p,p,p)^{abcd}_{\alpha\beta\gamma\delta} = \tag{B.5}$$
$$\left[S_{q_1}(p)^{-1}\right]^{aa'}_{\alpha\alpha'} \left[S_{q_3}(p)^{-1}\right]^{cc'}_{\gamma\gamma'} G_i(p,p,p,p)^{a'b'c'd'}_{\alpha'\beta'\gamma'\delta'} \left[S_{q_2}(p)^{-1}\right]^{b'b}_{\beta'\beta} \left[S_{q_4}(p)^{-1}\right]^{d'd}_{\delta'\delta}\,.$$

For the sake of clarity, we will use matrix notation, denoting the matrices by boldface symbols and omitting color and spin indices. The amputated Green functions will be collected in the 1×5 row vector

$$\boldsymbol{\Lambda}(p) = (\,\Lambda_1,\, \Lambda_2,\, \Lambda_3,\, \Lambda_4,\, \Lambda_5\,)\,(p,p,p,p)\,. \tag{B.6}$$

Setting

$$\hat{\boldsymbol{\Lambda}}(ap, a\mu) = Z_q^{-2}(ap)\, \boldsymbol{\Lambda}(ap)\, \left[\,\mathbf{I} + \boldsymbol{\Delta}^T\,\right] \mathbf{Z}(a\mu)^{\mathrm{T}}\,, \tag{B.7}$$

the renormalization matrix $\mathbf{Z}(a\mu)$ is determined by solving the renormalization conditions [51], namely

$$\mathbf{P}\,\hat{\boldsymbol{\Lambda}}(p)\,|_{p^2 = \mu^2} = \mathbf{I}\,. \tag{B.8}$$

In eq. (B.8), Z_q is the quark field RC and $\boldsymbol{\Delta}$ is, as we said before, the mixing matrix. We have also introduced the 5×1 column vector of spin projectors (see eq. (37) of ref. [51] for the explicit form of these projectors)

$$\mathbf{P}^{\mathrm{T}} = (\,P_1,\, P_2,\, P_3,\, P_4,\, P_5\,) \tag{B.9}$$

which act on the amputed Green functions by $(i, j = 1\cdots, 5)$,

$$P_i\, \Lambda_j \equiv \mathrm{Tr}\, P_i\, \Lambda_j(ap)$$

where the trace is taken over spin and colour, and obey the orthogonality relations

$$\mathrm{Tr}\, P_i\, \Lambda_j^{(0)}(ap) = \delta_{ij}\,, \tag{B.10}$$

with $\Lambda_j^{(0)}$ the tree level amputated Green function of the operator Q_j. It is convenient to express $\boldsymbol{\Lambda}$ in terms of a "dynamics" matrix $\mathbf{D}$, defined by

$$\boldsymbol{\Lambda}(ap) = \boldsymbol{\Lambda}^{(0)}(ap)\, \mathbf{D}(ap)\,. \tag{B.11}$$

This matrix equation can be solved for $\mathbf{D}$ using the spin projectors $\mathbf{P}$, getting

$$\mathbf{D}(p) \,=\, \mathbf{P}\,\mathbf{\Lambda}(p)\,. \tag{B.12}$$

Combining eqs. (B.7), (B.8) and (B.12), we see that, once the dynamics matrix is known, we can determine both the renormalization and the mixing matrices from the relation

$$Z_q^{-2}\,\mathbf{D}\,\left[\,\mathbf{I} + \mathbf{\Delta}^{\mathrm{T}}\,\right]\,\mathbf{Z}^{\mathrm{T}} \,=\, \mathbf{I} \,\to\, \mathbf{Z}\,\left[\,\mathbf{I} + \mathbf{\Delta}\,\right] \,=\, Z_q^2\,\left(\mathbf{D}^{\mathrm{T}}\right)^{-1}\,. \tag{B.13}$$

This matrix equation can be solved for $\mathbf{Z}$ and $\mathbf{\Delta}$ by exploiting the block diagonal structure of the $\mathbf{Z}$ matrix. In fact, it is easy to see that the three diagonal blocks of the renormalization matrix $(i, j = 1;\ i, j = 2, 3$ and $i, j = 4, 5)$ are given by

$$Z_{ij} \,=\, Z_q^2\,\left(\mathbf{D}^{\mathrm{T}}\right)_{ij}^{-1} \qquad (i, j = 1)\ \ (i, j = 2, 3)\ \ (i, j = 4, 5) \tag{B.14}$$

whereas the mixing coefficients are easily obtained from the equations,

$$Z_{11}\,\Delta_{1i} \,=\, Z_q^2\,\left(\mathbf{D}^{\mathrm{T}}\right)_{1i}^{-1} \qquad\qquad i = 2, \cdots, 5 \tag{B.15}$$

$$\begin{pmatrix} Z_{ii} & Z_{i\,i+1} \\ Z_{i+1\,i} & Z_{i+1\,i+1} \end{pmatrix} \begin{pmatrix} \Delta_{ij} \\ \Delta_{i+1\,j} \end{pmatrix} \,=\, Z_q^2\,\begin{pmatrix} \left(\mathbf{D}^{\mathrm{T}}\right)_{ij}^{-1} \\ \left(\mathbf{D}^{\mathrm{T}}\right)_{i+1\,i}^{-1} \end{pmatrix}\,\left\{\begin{matrix} i = 2\ j = 1, 4, 5 \\ i = 4\ j = 1, 2, 3 \end{matrix}\right\}\,.$$

We can now summarize our procedure to determine the renormalization matrix of the parity-even part of the four-fermion operators of the SUSY basis of eq. (2.2).

Step 1 The Green functions (B.4) and (B.5), and from them the dynamics matrix $\mathbf{D}$, are evaluated in the Landau gauge for a sequence of sea, μ_{sea}, and valence, μ_{val}, quark mass values at each of the four lattice spacings we consider here. The bare parameters and the statistics of this computation are detailed in table 2 of ref. [18]. One can also find there (see eqs. (3.6) and (3.7)) the set of discrete lattice momenta, p_ν $(p_{1,2,3} = (2\pi/L)\,n_{1,2,3},\ p_4 = (2\pi/T)\,(n_4 + 1/2))$, that we include in the present calculation. To minimize the contributions of Lorentz non-invariant discretization artifacts, we take into consideration only momenta satisfying the constraint

$$\sum_\rho \tilde{p}_\rho^4 \,<\, 0.28\,\left(\sum_\nu \tilde{p}_\nu^2\right)^2\,, \qquad a\,\tilde{p}_\nu \equiv \sin(a p_\nu)\,. \tag{B.16}$$

In the following, we shall often use the short-hand $\tilde{p}^2 = \sum_\nu \tilde{p}_\nu^2$.

Step 2 For each β and each choice of the scale $\tilde{p}^2$, the renormalization relation (B.14) is enforced at all values of μ_{sea} and μ_{val} given in table 2 of ref. [18]. By doing so, we obtain at nonzero quark masses the estimators $Z_{ij}^{\mathrm{RI}'}(\tilde{p}^2; a^2\tilde{p}^2; \mu_{\mathrm{val}}; \mu_{\mathrm{sea}})$, which are then extrapolated to $\mu_{\mathrm{val}} = 0$ (see section B.2) and $\mu_{\mathrm{sea}} = 0$ (see section B.3).

Step 3 Improved estimates of $Z_{ij}^{\mathrm{RI}'}(\tilde{p}^2; a^2\tilde{p}^2; 0; 0)$, are obtained by subtracting the perturbatively leading cutoff effects (see section B.4).

Step 4 Using the NLO continuum QCD evolution of the renormalization matrix $\mathbf{Z}$ calculated in refs. [15, 52], the first argument of $Z_{ij}^{\mathrm{RI}'}(\tilde{p}^2; a^2\tilde{p}^2; 0; 0)$ is brought to a reference scale μ_0^2. In this step, we assume that the scales $\tilde{p}^2$ and μ_0^2 are large enough to make NLO perturbation theory accurate. This is the same level of accuracy achieved in the determination of the Wilson coefficients.

Step 5 The residual $a^2\tilde{p}^2$ dependence in $Z_{ij}^{\mathrm{RI}'}(\mu_0^2; a^2\tilde{p}^2; 0; 0)$ is attributed to lattice artifacts, which we treat according to either the M1 or M2 methods, introduced in ref. [18] (see section B.6).

Step 6 In order to reduce the statistical error, the lattice RC estimators are averaged over two equivalent patterns of Wilson parameters (r_1, r_2, r_3, r_4), namely $(1, 1, 1, -1)$ and $(-1, -1, -1, 1)$, as well as over different lattice momenta corresponding to the same $\tilde{p}^2$. We have checked that performing these averages before or after taking the chiral limit leads to consistent results.

B.2 Valence chiral limit

In view of the relation (B.14) and since the extraction of Z_q (see ref. [18]) poses no particular problems, our discussion will be mainly focused here on the quark mass dependence of the dynamics matrix $\mathbf{D}$. At fixed values of β, $a^2\tilde{p}^2$ and $a\mu_{\mathrm{sea}}$, we fit the dynamics matrix elements D_{ij} to the ansatz

$$D_{ij}(p; \mu_{\mathrm{val}}; \mu_{\mathrm{sea}}) = A(\tilde{p}^2; \mu_{\mathrm{sea}}) + B(\tilde{p}^2; \mu_{\mathrm{sea}})\, \mu_{\mathrm{val}} + C(\tilde{p}^2; \mu_{\mathrm{sea}})/\mu_{\mathrm{val}}. \qquad (B.17)$$

Here we have introduced a term with a pole in $\mu_{\mathrm{val}} \sim m_{PS}^2$ to cope with the expected Goldstone boson (GB) pole contribution to the elements of the $\mathbf{D}$ matrix. The existence of such a GB-pole term can be understood as follows. At asymptotically large p^2, non-perturbative effects giving contributions potentially divergent in the chiral limit to the Green functions (B.4) do vanish and the latter turn out to be polynomial in the quark mass parameters [16]. At finite values of p^2, however, the contributions to (the spectral decomposition of) these Green functions from one-GB intermediate state with momentum q and mass m_{PS}, give rise to terms proportional to $(q^2 + m_{PS}^2)^{-1}$ and suppressed by some power of $1/p^2$. If several one-GB intermediate states contribute to the spectral representation of the Green functions (B.4) several terms, each behaving as $(q^2 + m_{PS}^2)^{-1}$ and suppressed by some power of $1/p^2$, will show up. These results follow straightforwardly from the "polology' study of the Green functions (see e.g. the discussion in the book [53]) or from the well known Lehmann-Symanzik-Zimmermann (LSZ) reduction formalism. Now, since in the Green functions (B.4) the four-fermion operator is inserted at zero four-momentum transfer ($q = 0$), one expects, from the time orderings where two quark fields can create from the vacuum a pseudoscalar (i.e. GB) one-particle state, a contribution proportional to $1/m_{PS}^2$, suppressed by some power of $1/p^2$. Similarly, from those time orderings where two quark fields create a GB-state and two further quark fields destroy another GB-state, contributions do arise that behave as $(1/m_{PS}^2)^2$ and are twice more strongly suppressed at large p^2.

In conclusion, by exploiting (along the lines of appendix A of ref. [16]) the large-p^2 behaviour of the matrix element[9] $\langle 0|\bar{q}_f(p)q_{f'}(-p)|P^{f'f}\rangle$ and taking also into consideration the four factors of $S_q(p)^{-1}$ that stem from the relations (B.5), one finds that the dynamics matrix D_{ij} contains GB-pole contributions of the following kinds:

$$
\begin{aligned}
D_{ij}^{\text{Single }12} &\sim P_i S_{q_1}^{-1}(p) S_{q_2}^{-1}(-p)\langle 0|\bar{q}_2 q_1|P^{12}\rangle \frac{1}{p^4 \left(M^{12}\right)^2} \langle P^{12}|Q_j(0)|q_3(p)\bar{q}_4(-p)\rangle \\
D_{ij}^{\text{Single }34} &\sim P_i\langle q_1(p)\bar{q}_2(-p)|Q_j(0)|P^{34}\rangle \frac{1}{\left(M^{34}\right)^2 p^4} \langle P^{34}|\bar{q}_4 q_3|0\rangle S_{q_3}^{-1}(p) S_{q_4}^{-1}(-p) \\
D_{ij}^{\text{Double }12\,34} &\sim P_i S_{q_1}^{-1}(p) S_{q_2}^{-1}(-p)\langle 0|\bar{q}_2 q_1|P^{12}\rangle \frac{\langle P^{12}|Q_j(0)|P^{34}\rangle}{p^4 \left(M^{12}\right)^2 \left(M^{34}\right)^2 p^4} \times \\
&\quad\times \langle P^{34}|\bar{q}_4 q_3|0\rangle S_{q_3}^{-1}(p) S_{q_4}^{-1}(-p).
\end{aligned}
\tag{B.18}
$$

We recall that the kinematics of our Green functions corresponds to an exceptional momentum configuration where $p_1 = p_3 = -p_2 = -p_4 = p$, and thus $q = 0$. As in the chiral limit $S_q^{-1}(p) \sim \gamma_\mu p_\mu$, the result (B.18) implies that single and double GB-pole terms are suppressed by $1/p^2$ and $1/(p^2)^2$ factors, respectively. A second observation is that thanks to the choice $r_4 = -r_3$ in our MA setup the lattice axial current $\bar{q}_4\gamma_\mu\gamma_5 q_3$ is conserved (only broken by soft mass terms) and hence the matrix elements of the operator Q_1 in $D_{i1}^{\text{Single }34}$ and $D_{i1}^{\text{Double }12\,34}$ vanish as $\left(M^{34}\right)^2 \sim (\mu_3 + \mu_4)$ in the limit $\mu_{3,4} \to 0$. This implies that no double pole occurs in D_{i1}. At non-vanishing lattice spacing there exists, however, an $\mathrm{O}(a^2)$ single pole contribution in $D_{i1}^{\text{Single }12}$ because, owing to $r_2 = r_1$, the lattice axial current $\bar{q}_2\gamma_\mu\gamma_5 q_1$ is broken by discretization effects (see ref. [11] and appendix A of ref. [8]).

For the case $j \neq 1$, when no similar GB-pole simplifications can occur, double GB-pole terms strongly suppressed (like $1/(p^2)^2$) at large p^2 are to be expected in $D_{ij}(p)$. However, precisely owing to this strong suppression in practice, within our statistical errors and in the ranges of quark masses and p^2 we explore (see table 2 of ref. [18] and section B.6), we hardly see in our lattice data any effects that can reliably be ascribed to double GB-pole contributions. On the contrary, we do find clear numerical evidence for single GB-pole contributions, which indeed at high p^2 are only suppressed as $1/p^2$. We thus decided to ignore double GB-pole terms in our valence mass chiral extrapolations.

This choice is also justified a posteriori by the results of the valence chiral fits based on the ansatz (B.17). A subset of these results is illustrated in figure 6. There we display typical examples of the effect of GB-pole subtractions in the matrix elements of the dynamics matrix at two values of β. As can be seen, after the subtraction, a smooth dependence upon μ_{val} (or equivalently on M_{12}^2) is observed. Combining the valence chiral limit lattice estimator of D_{ij} and Z_q, we are able to get reliable estimates of the intermediate quantities $Z_{ij}^{\text{lat}}(\tilde{p}^2; a^2\tilde{p}^2; 0, a\mu_{\text{sea}})$.

---

[9]Here $q'_f(p)$ $(\bar{q}_f(p))$ denotes the four-dimensional Fourier transform of the quark field $q'_f(x)$ $(\bar{q}_f(x))$, while $|P^{f'f}\rangle$ is the pseudoscalar meson state with valence quarks of flavour f and f'.
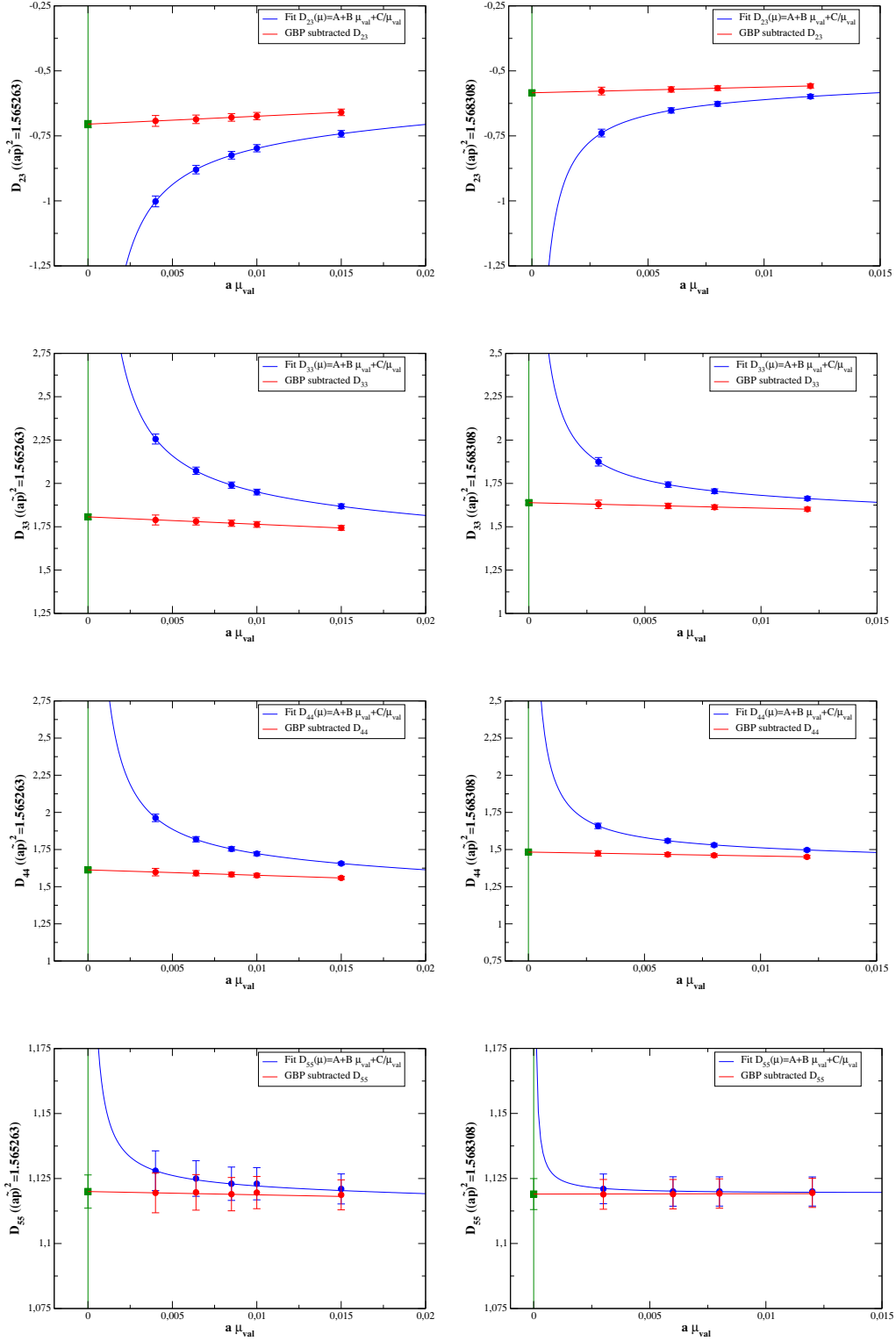
Figure 6. GB-pole subtraction and valence chiral limit of D_{23}, D_{33}, D_{44} and D_{55} plotted versus $a\mu_{\text{val}}$, for $\beta = 3.9$, $a\mu_{\text{sea}} = 0.0040$ and $(a\tilde{p})^2 \approx 1.565$ (left column) and $\beta = 4.05$, $a\mu_{\text{sea}} = 0.0030$ and $(a\tilde{p})^2 \approx 1.568$ (right column).
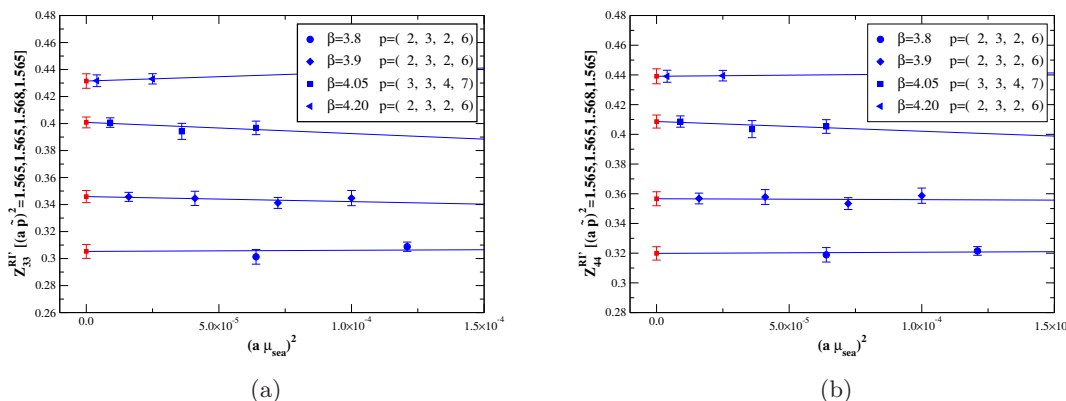
Figure 7. The quantities $Z_{33}^{\mathrm{RI}'}(\tilde{p}^2; a^2\tilde{p}^2; 0, a\mu_{\mathrm{sea}})$ and $Z_{44}^{\mathrm{RI}'}(\tilde{p}^2; a^2\tilde{p}^2; 0, a\mu_{\mathrm{sea}})$, taken at the valence chiral limit, as functions of $a^2\mu_{\mathrm{sea}}^2$, for a typical lattice momentum choice (see inset) giving $a^2\tilde{p}^2 \sim 1.56$, for four β values ($\beta =3.80$, 3.90, 4.05 and 4.20).

B.3 Sea chiral limit

At fixed β and $a^2\tilde{p}^2$, we fit $Z_{ij}^{\mathrm{lat}}(\tilde{p}^2; a^2\tilde{p}^2; 0, a\mu_{\mathrm{sea}})$ data to a first order polynomial in $a^2\mu_{\mathrm{sea}}^2$. This choice is dictated by the expectation that effects of spontaneous chiral symmetry, which may induce a dependence on $|\mu_{\mathrm{sea}}|$, are strongly suppressed, and in practice immaterial within errors, in quantities like our RC-estimators that are evaluated at momentum scales $\tilde{p}^2 \gg \Lambda_{\mathrm{QCD}}^2$. In fact we find that the dependence on the sea quark mass is hardly visible within our statistical error bars, as shown in figure 7. Moreover, we have checked that repeating the whole analysis using a constant fit leads to similar RC results, though affected by smaller errors and often, but not always, yielding acceptable χ^2's. Hence, we conservatively decided to perform the sea chiral extrapolation using a linear fit in $a^2\mu_{\mathrm{sea}}^2$. We construct in this way the RC estimators $Z_{ij}^{\mathrm{RI}'}(\tilde{p}^2; a^2\tilde{p}^2; 0, 0)$.

B.4 Removal of $O(a^2g^2)$ cutoff effects

We will obtain improved chiral limit RC estimators, $Z_{ij}^{\mathrm{RI}'-\mathrm{impr}}(\tilde{p}^2; a^2\tilde{p}^2)$, by removing from our $Z_{ij}^{\mathrm{RI}'}(\tilde{p}^2; a^2\tilde{p}^2; 0, 0)$ lattice data perturbative discretization errors. This can be done up to $O(a^2g^2)$ exploiting the one-loop perturbative results obtained [54, 55] in the massless lattice theory for the quark propagator form factor Σ_1, related to the quark-field RC by $Z_q(p) = \Sigma_1(p)$, and the dynamics matrix elements, *v.i.z.*

$$[\, Z_q(p)\,]^{\mathrm{LPT}} = 1 + \frac{g^2}{16\pi^2}a^2\left[\tilde{p}^2\left(c_q^{(1)} + c_q^{(2)}\log(a^2\tilde{p}^2)\right) + c_q^{(3)}\frac{\sum_\rho \tilde{p}_\rho^4}{\tilde{p}^2}\right] + \mathrm{O}(a^4g^2, g^4)$$

$$[\, D_{ij}(p)\,]^{\mathrm{LPT}} = 1 + \frac{g^2}{16\pi^2}\left[b_{ij}^{(1)} + b_{ij}^{(2)}\log(a^2\tilde{p}^2)\right] \tag{B.19}$$

$$+ \frac{g^2}{16\pi^2}a^2\left[\tilde{p}^2\left(c_{ij}^{(1)} + c_{ij}^{(2)}\log(a^2\tilde{p}^2)\right) + c_{ij}^{(3)}\frac{\sum_\rho \tilde{p}_\rho^4}{\tilde{p}^2}\right] + \mathrm{O}(a^4g^2, g^4)$$
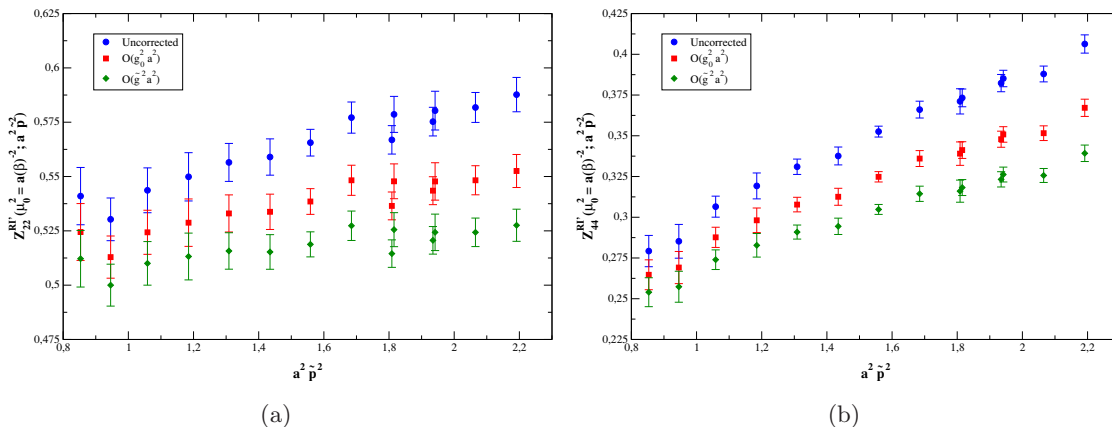
Figure 8. The effect of subtracting from $Z_{22}^{\mathrm{RI'}}(\mu_0^2 = a(\beta)^{-2}; a^2\tilde{p}^2; 0, 0)$ and $Z_{44}^{\mathrm{RI'}}(\mu_0^2 = a(\beta)^{-2}; a^2\tilde{p}^2; 0, 0)$ at $\beta = 3.8$ (blue dots) the $\mathrm{O}(a^2 g^2)$ correction, setting either $g^2 = g_0^2$ (red squares) or $g^2 = \tilde{g}^2$ (green diamonds).

The values of the coefficients $c_q^{(k)}$, $k = 1, 2, 3$ can be found in eq. (34) of ref. [18], while the values of the coefficients $b_{ij}^{(k)}$ and $c_{ij}^{(k)}$ are available in refs. [54, 55].

In the numerical evaluation of the perturbative corrections, we take the coupling constant g^2 as the simple boosted coupling $\tilde{g}^2 \equiv g_0^2/\langle P \rangle$. For the average plaquette $\langle P \rangle$ we employ the non-perturbative values $[0.5689, 0.5825, 0.6014, 0.6200]$ corresponding to $\beta = [3.8, 3.9, 4.05, 4.20]$, respectively. The important impact of the perturbative corrections in removing the unwanted $a^2\tilde{p}^2$ dependence is illustrated, for the case of $\beta = 3.8$, in figure 8. In this figure, the uncorrected values of $Z_{ij}^{\mathrm{RI'}}(\mu_0^2 = a(\beta)^{-2}; a^2\tilde{p}^2; 0, 0)$ are compared with the values of $Z_{ij}^{\mathrm{RI'-impr}}(\mu_0^2 = a(\beta)^{-2}; a^2\tilde{p}^2)$ obtained setting either $g^2 = g_0^2 = 6/\beta$ or (as we did in the end) $g^2 = \tilde{g}^2$.

B.5 Absence of wrong chirality mixings

In figure 9, one can clearly see that for all the operators of interest the mixing coefficients Δ_{ij} are very small (in fact vanishing within errors in the range of $\tilde{p}^2$ that we eventually use for extracting RCs). We also find that this is systematically more and more so as β increases, well in line with our expectation that in our lattice setup wrong chirality mixing effects are reduced to mere $\mathrm{O}(a^2)$ artifacts. For these reasons the effects of $\boldsymbol{\Delta}$ have been neglected in our final RC analysis, where we have assumed a fully continuum-like relation between renormalized and bare operators. In addition we checked that repeating the whole analysis with the tiny effects of $\boldsymbol{\Delta}$ on the relation (B.1) properly taken into account leads to no significant changes in the values of RCs.

B.6 Final RC estimates from M1 and M2 method

Having extrapolated the (improved) RCs estimators to the valence and sea chiral limit at each value of the momenta, we evolve $Z_{ij}^{\mathrm{RI'-impr}}(\tilde{p}^2; a^2\tilde{p}^2)$ from the scale $\tilde{p}^2$ to a common scale μ_0^2 by using the known matrix formula for the NLO running of the operators Q_i [15, 52], obtaining $Z_{ij}^{\mathrm{RI'-impr}}(\mu_0^2; a^2\tilde{p}^2)$. This step is necessary in order to disentangle
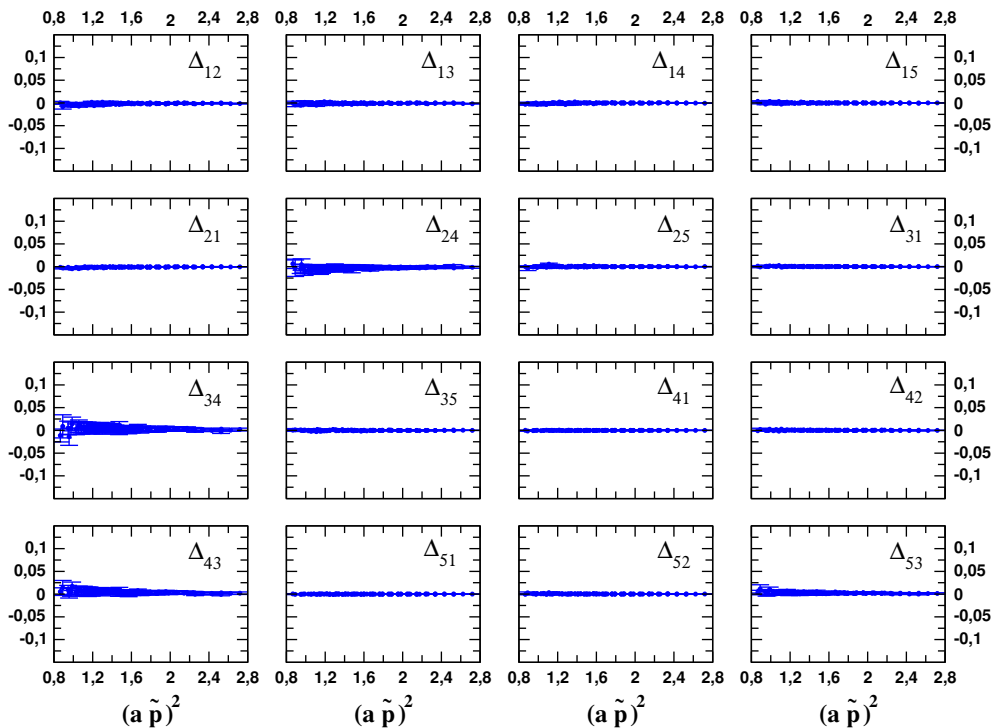
Figure 9. The behaviour of the mixing coefficients Δ_{ij}, as a function of $a^2\tilde{p}^2$ for $\beta = 4.05$.

the $\mathrm{O}(a^2\tilde{p}^2)$ cutoff effects from the genuine continuum p^2 dependence. Notice also that the actual value of μ_0 has no impact on the RGI results of the RC's. As is customary, we take $\mu_0 = a^{-1}(\beta)$ for each β, with $a^{-1}(3.8, 3.9, 4.05, 4.20) = [2.0, 2.3, 3.0, 3.7]\,\mathrm{GeV}$.

Of course we still allow for a residual dependence on $a^2\tilde{p}^2$. In order to deal with these cutoff effects, following ref. [18], we use two methods. Method M1 consists in fitting $Z_{ij}^{\mathrm{RI}'-\mathrm{impr}}(\mu_0^2; a^2\tilde{p}^2)$ to the linear ansatz

$$Z_{ij}^{\mathrm{RI}'-\mathrm{impr}}(\mu_0^2; a^2\tilde{p}^2) = Z_{ij}^{\mathrm{RI}'-\mathrm{impr}}(\mu_0^2) + \lambda_{ij}\,(a\tilde{p})^2 \tag{B.20}$$

in the large momentum region, $1.0 \leq a^2\tilde{p}^2 \leq 2.2$. As expected, the slopes λ_{ij} depend smoothly on β.

According to the ansatz (B.20), with $\lambda_{ij} = \lambda_{ij}^{(0)} + \lambda_{ij}^{(1)}\tilde{g}^2$ ($\tilde{g}^2$ is the boosted gauge coupling as in section B.4) a linear extrapolation to $a^2\tilde{p}^2 = 0$ was performed simultaneously at all β's. The extrapolated values, $Z_{ij}^{\mathrm{RI}'-\mathrm{impr}}(\mu_0^2)$, are finally used to evaluate via the NLO running matrix formula of ref. [15], the quantities $Z_{ij}^{\overline{\mathrm{MS}}}(M1)$ and $Z_{ij}^{\mathrm{RGI}}(M1)$. Therefore, the $\overline{\mathrm{MS}}$ scheme we use here is the one defined by Buras et al. in ref. [15]. This definition of the $\overline{\mathrm{MS}}$ scheme, which has become standard, differs from the one of ref. [52] proposed by Ciuchini et al. in the treatment of the four-fermion evanescent operators appearing in the calculation of the two-loop anomalous dimensions.

In figure 10 the simultaneous best linear fits in $a^2\tilde{p}^2$ at our four β's of Z_{ij} are shown. We recall that both in the analysis and in the figures of this appendix, only data points corresponding to the momenta $\tilde{p}$ satisfying the constraint (B.16) are used and shown.
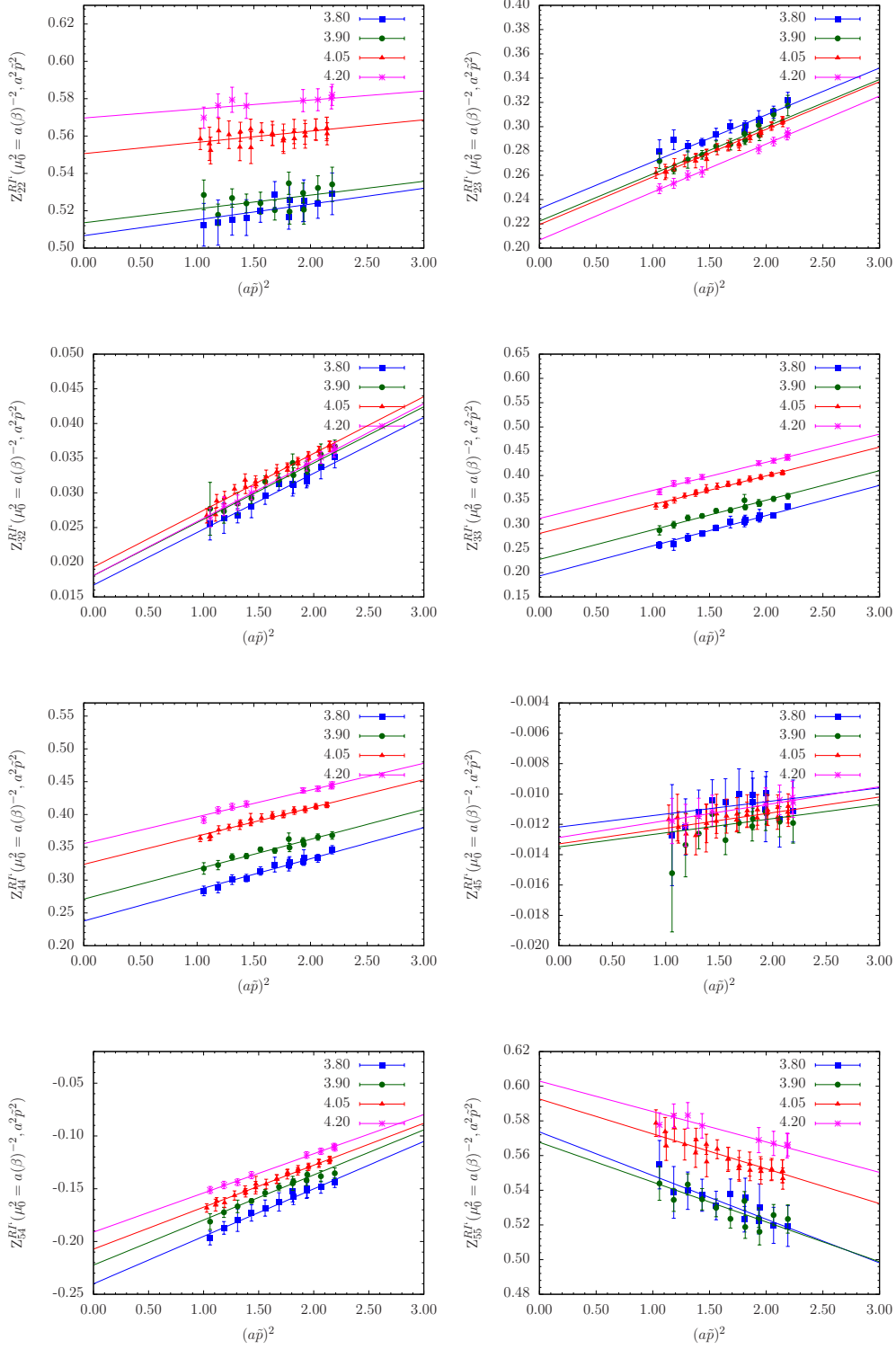
Figure 10. $Z_{ij}^{\mathrm{RI'-impr}}(\mu_0^2 = a(\beta)^{-2}; a^2\,\tilde{p}^2)$ for $\{ij\} = \{22, 23, 32, 33, 44, 45, 54, 55\}$ as functions of $a^2\,\tilde{p}^2$ for the four β values considered in our study. The straight lines represent the simultaneous linear fit to the lattice data in the interval $1.0 \le a^2\tilde{p}^2 \le 2.2$ at the four β's.

RC(M1)	$\beta = 3.80$	$\beta = 3.90$	$\beta = 4.05$	$\beta = 4.20$
$\overline{\text{MS}}$ at $2\,\text{GeV}$				
Z_P	0.413(12)	0.437(7)	0.477(6)	0.498(5)
Z_S	0.728(16)	0.712(10)	0.702(5)	0.694(8)
RI-MOM at $2\,\text{GeV}$				
Z_P	0.339(9)	0.359(6)	0.391(4)	0.409(4)
Z_S	0.598(13)	0.585(9)	0.576(4)	0.570(7)

Table 7. Z_P and Z_S results, using the M1 method at $\beta = 3.80$, 3.90, 4.05 and 4.20 in $\overline{\text{MS}}$ and RI-MOM at $2\,\text{GeV}$.

RC(M2)	$\beta = 3.80$	$\beta = 3.90$	$\beta = 4.05$	$\beta = 4.20$
$\overline{\text{MS}}$ at $2\,\text{GeV}$				
Z_P	0.532(5)	0.518(6)	0.520(4)	0.503(5)
Z_S	0.813(7)	0.776(6)	0.735(4)	0.708(10)
RI-MOM at $2\,\text{GeV}$				
Z_P	0.437(4)	0.426(5)	0.427(4)	0.413(4)
Z_S	0.668(6)	0.637(5)	0.603(4)	0.582(8)

Table 8. Z_P and Z_S results, using the M2 method, at $\beta =$3.80, 3.90, 4.05 and 4.20 in $\overline{\text{MS}}$ and RI-MOM at $2\,\text{GeV}$.

The idea of the M2 method is instead to separately average at each β the values of $Z_{ij}^{\text{RI}'-\text{impr}}(\mu_0^2; a^2\tilde{p}^2)$ over a narrow interval of momenta (ideally just one point), which has to be kept fixed in physical units for all β's. We have chosen this interval to be $\tilde{p}^2 \in [\,8.0,\, 9.5\,]\,\text{GeV}^2$. In this way, at the price of giving up the reduction of cutoff effects implied by the M1 method, no assumptions are introduced in the RC analysis about the detailed form of lattice artifacts and/or the adequacy of NLO anomalous dimensions to describe the RC-evolution at scales below $\tilde{p}^2 \sim 9\,\text{GeV}^2$.

The a^2-scaling of renormalized quantities (in this work operator matrix elements) constructed using RCs determined with the M2 method will of course be in general different from the one of their M1 method counterparts, but the continuum limit results for these quantities, if attainable from both methods with controlled errors, should be consistent with each other (see e.g. appendix E).

C   Renormalization constant results

In tables 7 and 8 we collect values of Z_P and Z_S calculated in the RI-MOM scheme. Results are obtained with methods M1 and M2 [18] at each value of the gauge coupling in $\overline{\text{MS}}$ and RI-MOM at $2\,\text{GeV}$. We have used the three-loop conversion formula from RI-MOM to $\overline{\text{MS}}$ [56].

The RC matrices of the four-fermion operators Z_Q, (cf. eq. (A.10)), are listed below. We present results obtained from both M1 and M2 methods, in $\overline{\text{MS}}$ and RI-MOM at $2\,\text{GeV}$.

$(\overline{\text{MS}},\ 2\,\text{GeV})$:

$$Z_Q(\beta = 3.80; M1) = \begin{pmatrix} 0.425(15) & 0 & 0 & 0 & 0 \\ 0 & 0.493(12) & 0.207(7) & 0 & 0 \\ 0 & 0.022(02) & 0.226(10) & 0 & 0 \\ 0 & 0 & 0 & 0.257(9) & -0.006(2) \\ 0 & 0 & 0 & -0.246(8) & 0.600(14) \end{pmatrix}$$

$$Z_Q(\beta = 3.90; M1) = \begin{pmatrix} 0.441(8) & 0 & 0 & 0 & 0 \\ 0 & 0.505(9) & 0.206(7) & 0 & 0 \\ 0 & 0.023(1) & 0.250(6) & 0 & 0 \\ 0 & 0 & 0 & 0.282(6) & -0.006(2) \\ 0 & 0 & 0 & -0.244(5) & 0.617(11) \end{pmatrix}$$

$$Z_Q(\beta = 4.05; M1) = \begin{pmatrix} 0.491(5) & 0 & 0 & 0 & 0 \\ 0 & 0.550(6) & 0.223(5) & 0 & 0 \\ 0 & 0.024(1) & 0.282(5) & 0 & 0 \\ 0 & 0 & 0 & 0.319(4) & -0.004(1) \\ 0 & 0 & 0 & -0.258(5) & 0.692(8) \end{pmatrix}$$

$$Z_Q(\beta = 4.20; M1) = \begin{pmatrix} 0.523(10) & 0 & 0 & 0 & 0 \\ 0 & 0.575(9) & 0.227(6) & 0 & 0 \\ 0 & 0.023(1) & 0.294(9) & 0 & 0 \\ 0 & 0 & 0 & 0.336(7) & -0.002(2) \\ 0 & 0 & 0 & -0.265(6) & 0.727(10) \end{pmatrix}$$

$(\overline{\text{MS}},\ 2\,\text{GeV})$:

$$Z_Q(\beta = 3.80; M2) = \begin{pmatrix} 0.440(9) & 0 & 0 & 0 & 0 \\ 0 & 0.512(7) & 0.272(5) & 0 & 0 \\ 0 & 0.043(2) & 0.382(5) & 0 & 0 \\ 0 & 0 & 0 & 0.367(5) & -0.005(2) \\ 0 & 0 & 0 & -0.148(4) & 0.547(9) \end{pmatrix}$$

$$Z_Q(\beta = 3.90; M2) = \begin{pmatrix} 0.447(5) & 0 & 0 & 0 & 0 \\ 0 & 0.514(5) & 0.260(4) & 0 & 0 \\ 0 & 0.038(1) & 0.362(4) & 0 & 0 \\ 0 & 0 & 0 & 0.361(4) & -0.005(1) \\ 0 & 0 & 0 & -0.169(3) & 0.576(5) \end{pmatrix}$$

$$Z_Q(\beta = 4.05; M2) = \begin{pmatrix} 0.495(5) & 0 & 0 & 0 & 0 \\ 0 & 0.555(5) & 0.264(4) & 0 & 0 \\ 0 & 0.033(1) & 0.343(4) & 0 & 0 \\ 0 & 0 & 0 & 0.360(3) & -0.003(1) \\ 0 & 0 & 0 & -0.214(4) & 0.663(8) \end{pmatrix}$$

$$Z_Q(\beta = 4.20; M2) = \begin{pmatrix} 0.531(6) & 0 & 0 & 0 & 0 \\ 0 & 0.588(6) & 0.278(3) & 0 & 0 \\ 0 & 0.026(1) & 0.304(5) & 0 & 0 \\ 0 & 0 & 0 & 0.337(5) & -0.000(1) \\ 0 & 0 & 0 & -0.259(4) & 0.733(8) \end{pmatrix}$$

(RI-MOM, 2 GeV):

$$Z_Q(\beta = 3.80; M1) = \begin{pmatrix} 0.419(15) & 0 & 0 & 0 & 0 \\ 0 & 0.506(13) & 0.233(7) & 0 & 0 \\ 0 & 0.017(2) & 0.194(9) & 0 & 0 \\ 0 & 0 & 0 & 0.238(8) & -0.013(2) \\ 0 & 0 & 0 & -0.240(8) & 0.574(14) \end{pmatrix}$$

$$Z_Q(\beta = 3.90; M1) = \begin{pmatrix} 0.434(8) & 0 & 0 & 0 & 0 \\ 0 & 0.517(9) & 0.236(7) & 0 & 0 \\ 0 & 0.018(1) & 0.215(5) & 0 & 0 \\ 0 & 0 & 0 & 0.261(6) & -0.013(1) \\ 0 & 0 & 0 & -0.239(5) & 0.589(11) \end{pmatrix}$$

$$Z_Q(\beta = 4.05; M1) = \begin{pmatrix} 0.483(5) & 0 & 0 & 0 & 0 \\ 0 & 0.563(6) & 0.256(5) & 0 & 0 \\ 0 & 0.019(1) & 0.242(4) & 0 & 0 \\ 0 & 0 & 0 & 0.295(3) & -0.012(1) \\ 0 & 0 & 0 & -0.253(5) & 0.659(8) \end{pmatrix}$$

$$Z_Q(\beta = 4.20; M1) = \begin{pmatrix} 0.515(10) & 0 & 0 & 0 & 0 \\ 0 & 0.589(9) & 0.261(7) & 0 & 0 \\ 0 & 0.018(1) & 0.253(7) & 0 & 0 \\ 0 & 0 & 0 & 0.311(7) & -0.011(1) \\ 0 & 0 & 0 & -0.260(6) & 0.694(10) \end{pmatrix}$$

(RI-MOM, 2 GeV):

$$Z_Q(\beta = 3.80; M2) = \begin{pmatrix} 0.433(8) & 0 & 0 & 0 & 0 \\ 0 & 0.527(7) & 0.318(5) & 0 & 0 \\ 0 & 0.034(1) & 0.324(4) & 0 & 0 \\ 0 & 0 & 0 & 0.338(4) & -0.011(2) \\ 0 & 0 & 0 & -0.149(4) & 0.522(9) \end{pmatrix}$$

$$Z_Q(\beta = 3.90; M2) = \begin{pmatrix} 0.441(4) & 0 & 0 & 0 & 0 \\ 0 & 0.528(5) & 0.304(4) & 0 & 0 \\ 0 & 0.031(1) & 0.307(4) & 0 & 0 \\ 0 & 0 & 0 & 0.332(3) & -0.012(1) \\ 0 & 0 & 0 & -0.169(3) & 0.550(5) \end{pmatrix}$$

$$Z_Q(\beta = 4.05; M2) = \begin{pmatrix} 0.487(5) & 0 & 0 & 0 & 0 \\ 0 & 0.570(5) & 0.306(5) & 0 & 0 \\ 0 & 0.026(1) & 0.291(3) & 0 & 0 \\ 0 & 0 & 0 & 0.331(3) & -0.011(1) \\ 0 & 0 & 0 & -0.212(4) & 0.632(8) \end{pmatrix}$$

$$Z_Q(\beta = 4.20; M2) = \begin{pmatrix} 0.523(6) & 0 & 0 & 0 & 0 \\ 0 & 0.602(6) & 0.314(4) & 0 & 0 \\ 0 & 0.020(1) & 0.261(4) & 0 & 0 \\ 0 & 0 & 0 & 0.308(4) & -0.009(1) \\ 0 & 0 & 0 & -0.254(4) & 0.700(7) \end{pmatrix}$$

D   Lattice data on masses and matrix elements

In the following tables we gather our bare results at all values of β and combinations of quark masses for (i) pseudoscalar meson masses and pseudoscalar meson decay constants in lattice units (tables 9, 10, 11 and 12); (ii) the ratio of the (bare) four-fermion operators $R_i^{(b)} = \langle \bar{K}^0 | O_i | K^0 \rangle / \langle \bar{K}^0 | O_1 | K^0 \rangle$ ($i = 2, \ldots, 5$) (see tables 13, 14, 15 and 16); (iii) the quantities $\xi_i \, B_i^{(0)}$ ($i = 2, \ldots, 5$) (see tables 17, 18, 19 and 20).

$\beta = 3.80$ $(24^3 \times 48)a^4$					
$a\mu_\ell = a\mu_{\text{sea}}$	$a\mu_{\text{"}s\text{"}}$	aM^{34}	aM^{12}	aF^{34}	aF^{12}
	0.0165	0.2558(8)	0.3393(25)	0.0894(4)	0.0883(15)
0.0080	0.0200	0.2731(7)	0.3532(23)	0.0913(4)	0.0895(15)
	0.0250	0.2961(7)	0.3718(21)	0.0936(4)	0.0909(15)
	0.0165	0.2712(4)	0.3508(16)	0.0924(3)	0.0900(16)
0.0110	0.0200	0.2877(4)	0.3644(14)	0.0942(3)	0.0910(16)
	0.0250	0.3098(4)	0.3828(12)	0.0966(3)	0.0924(16)

Table 9. Pseudoscalar masses and decay constants at $\beta = 3.80$.

$\beta = 3.90$ $(24^3 \times 48)a^4$					
$a\mu_\ell = a\mu_{\text{sea}}$	$a\mu_{\text{"}s\text{"}}$	aM^{34}	aM^{12}	aF^{34}	aF^{12}
	0.0150	0.2060(5)	0.2639(11)	0.0724(3)	0.0705(9)
0.0040	0.0220	0.2401(5)	0.2915(11)	0.0757(3)	0.0725(9)
	0.0270	0.2619(5)	0.3096(11)	0.0777(3)	0.0759(9)
	0.0150	0.2179(8)	0.2762(16)	0.0755(5)	0.0736(10)
0.0064	0.0220	0.2506(7)	0.3028(15)	0.0785(5)	0.0759(9)
	0.0270	0.2717(7)	0.3204(14)	0.0805(4)	0.0774(9)
	0.0150	0.2283(7)	0.2849(17)	0.0773(3)	0.0755(9)
0.0085	0.0220	0.2598(7)	0.3109(15)	0.0804(3)	0.0779(8)
	0.0270	0.2803(7)	0.3281(15)	0.0823(3)	0.0794(9)
	0.0150	0.2351(7)	0.2892(14)	0.0784(4)	0.0761(9)
0.0100	0.0220	0.2659(7)	0.3154(12)	0.0815(4)	0.0787(8)
	0.0270	0.2860(6)	0.3328(12)	0.0834(4)	0.0802(9)
$\beta = 3.90$ $(32^3 \times 64)a^4$					
	0.0150	0.1982(4)	0.2558(13)	0.0720(3)	0.0701(7)
0.0030	0.0220	0.2329(4)	0.2838(11)	0.0750(3)	0.0720(8)
	0.0270	0.2550(4)	0.3021(11)	0.0770(3)	0.0745(8)
	0.0150	0.2041(4)	0.2644(15)	0.0727(3)	0.0702(11)
0.0040	0.0220	0.2381(4)	0.2917(17)	0.0758(3)	0.0722(10)
	0.0270	0.2599(4)	0.3096(15)	0.0777(3)	0.0753(9)

Table 10. Pseudoscalar masses and decay constants at $\beta = 3.90$.

$\beta = 4.05\ (32^3 \times 64)a^4$					
$a\mu_\ell = a\mu_{\text{sea}}$	$a\mu_{\text{“}s\text{”}}$	aM^{34}	aM^{12}	aF^{34}	aF^{12}
	0.0120	0.1602(8)	0.1931(18)	0.0564(3)	0.0558(7)
0.0030	0.0150	0.1751(8)	0.2053(17)	0.0578(3)	0.0566(7)
	0.0180	0.1889(8)	0.2169(16)	0.0591(3)	0.0573(7)
	0.0120	0.1739(6)	0.2034(11)	0.0600(4)	0.0585(8)
0.0060	0.0150	0.1877(6)	0.2153(11)	0.0613(3)	0.0596(8)
	0.0180	0.2007(6)	0.2266(11)	0.0625(3)	0.0605(8)
	0.0120	0.1840(5)	0.2127(9)	0.0615(4)	0.0604(12)
0.0080	0.0150	0.1972(5)	0.2242(9)	0.0627(4)	0.0616(12)
	0.0180	0.2097(5)	0.2351(9)	0.0638(4)	0.0626(12)

Table 11. Pseudoscalar masses and decay constants at $\beta = 4.05$.

$\beta = 4.20\ (48^3 \times 96)a^4$					
$a\mu_\ell = a\mu_{\text{sea}}$	$a\mu_{\text{“}s\text{”}}$	aM^{34}	aM^{12}	aF^{34}	aF^{12}
	0.0116	0.1277(8)	0.1433(20)	0.0446(3)	0.0438(9)
0.0020	0.0129	0.1397(8)	0.1536(19)	0.0456(3)	0.0445(9)
	0.0142	0.1509(9)	0.1633(19)	0.0465(4)	0.0452(9)
$\beta = 4.20\ (32^3 \times 64)a^4$					
	0.0116	0.1522(11)	0.1682(20)	0.0483(5)	0.0476(8)
0.0065	0.0129	0.1628(10)	0.1777(18)	0.0494(5)	0.0486(7)
	0.0142	0.1729(10)	0.1868(17)	0.0503(5)	0.0495(7)

Table 12. Pseudoscalar masses and decay constants at $\beta = 4.20$.

$\beta = 3.80\ (24^3 \times 48)a^4$					
$a\mu_\ell = a\mu_{\text{sea}}$	$a\mu_{\text{“}s\text{”}}$	$-R_2^{(b)}$	$R_3^{(b)}$	$R_4^{(b)}$	$R_5^{(b)}$
	0.0165	13.14(7)	3.19(2)	24.29(12)	8.18(4)
0.0080	0.0200	11.92(6)	2.89(1)	21.93(10)	7.43(3)
	0.0250	10.58(4)	2.56(1)	19.34(8)	6.61(3)
	0.0165	12.16(6)	2.95(1)	21.89(10)	7.41(3)
0.0110	0.0200	11.15(5)	2.70(1)	19.99(8)	6.81(3)
	0.0250	9.99(4)	2.41(1)	17.84(7)	6.13(2)

Table 13. $R_i^{(b)}$ for $i = 2, \ldots, 5$, as obtained from eq. (4.17), at each combination of the quark mass pair $(a\mu_\ell, a\mu_{\text{“}s\text{”}})$ and at $\beta = 3.80$.

$\beta = 3.90 \ (24^3 \times 48)a^4$					
$a\mu_\ell = a\mu_{\text{sea}}$	$a\mu_{\text{“}s\text{”}}$	$-R_2^{(b)}$	$R_3^{(b)}$	$R_4^{(b)}$	$R_5^{(b)}$
	0.0150	16.42(6)	4.15(1)	32.51(12)	10.79(4)
0.0040	0.0220	13.11(4)	3.20(1)	24.99(7)	8.41(2)
	0.0270	11.38(3)	2.77(1)	21.57(6)	7.32(2)
	0.0150	15.37(8)	3.77(2)	29.02(14)	9.68(4)
0.0064	0.0220	12.21(5)	2.98(1)	22.89(9)	7.75(3)
	0.0270	10.70(4)	2.60(1)	19.97(7)	6.82(2)
	0.0150	14.10(5)	3.44(1)	26.56(9)	8.92(3)
0.0085	0.0220	11.41(3)	2.77(1)	21.32(6)	7.25(2)
	0.0270	10.09(3)	2.45(1)	18.75(5)	6.44(1)
	0.0150	13.52(5)	3.31(1)	25.30(9)	8.53(3)
0.0100	0.0220	11.07(4)	2.70(1)	20.55(6)	7.02(2)
	0.0270	9.85(3)	2.39(1)	18.28(5)	6.26(2)
$\beta = 3.90 \ (32^3 \times 64)a^4$					
	0.0150	17.18(8)	4.22(2)	33.45(14)	11.09(5)
0.0030	0.0220	13.27(5)	3.24(1)	25.66(12)	8.63(3)
	0.0270	11.47(5)	2.80(1)	22.09(9)	7.50(3)
	0.0150	16.32(9)	4.10(2)	32.22(18)	10.68(6)
0.0040	0.0220	13.01(6)	3.17(1)	24.88(12)	8.34(4)
	0.0270	11.31(5)	2.74(1)	21.42(9)	7.27(3)

Table 14. $R_i^{(b)}$ for $i = 2, \ldots, 5$, as obtained from eq. (4.17), at each combination of the quark mass pair $(a\mu_\ell, a\mu_{\text{“}s\text{”}})$ and at $\beta = 3.90$.

$\beta = 4.05 \ (32^3 \times 64)a^4$					
$a\mu_\ell = a\mu_{\text{sea}}$	$a\mu_{\text{“}s\text{”}}$	$-R_2^{(b)}$	$R_3^{(b)}$	$R_4^{(b)}$	$R_5^{(b)}$
	0.0120	20.47(12)	5.07(3)	40.49(22)	13.32(7)
0.0030	0.0150	17.35(9)	4.29(2)	34.29(17)	11.36(6)
	0.0180	15.10(7)	3.72(2)	29.78(13)	9.93(4)
	0.0120	16.61(9)	4.11(2)	32.49(15)	10.79(5)
0.0060	0.0150	14.55(7)	3.59(2)	28.35(11)	9.48(4)
	0.0180	12.97(5)	3.20(2)	25.19(9)	8.48(3)
	0.0120	15.13(5)	3.74(1)	29.36(9)	9.79(3)
0.0080	0.0150	13.42(4)	3.31(1)	25.99(7)	8.72(2)
	0.0180	12.09(3)	2.97(1)	23.34(6)	7.88(2)

Table 15. $R_i^{(b)}$ for $i = 2, \ldots, 5$, as obtained from eq. (4.17), at each combination of the quark mass pair $(a\mu_\ell, a\mu_{\text{“}s\text{”}})$ and at $\beta = 4.05$.

$\beta = 4.20\ (48^3 \times 96)a^4$					
$a\mu_\ell = a\mu_{\rm sea}$	$a\mu_{``s"}$	$-R_2^{(b)}$	$R_3^{(b)}$	$R_4^{(b)}$	$R_5^{(b)}$
	0.0116	21.56(12)	5.28(3)	44.37(25)	14.56(8)
0.0020	0.0129	18.28(9)	4.56(2)	37.52(20)	12.43(7)
	0.0142	15.88(8)	3.95(2)	32.57(17)	10.86(6)
$\beta = 4.20\ (32^3 \times 64)a^4$					
	0.0116	17.87(25)	4.46(6)	34.83(33)	11.57(11)
0.0065	0.0129	15.52(20)	3.87(5)	30.31(27)	10.13(9)
	0.0142	13.75(16)	3.42(4)	26.85(23)	9.03(7)

Table 16. $R_i^{(b)}$ for $i = 2, \ldots, 5$, as obtained from eq. (4.17), at each combination of the quark mass pair $(a\mu_\ell, a\mu_{``s"})$ and at $\beta = 4.20$.

$\beta = 3.80\ (24^3 \times 48)a^4$					
$a\mu_\ell = a\mu_{\rm sea}$	$a\mu_{``s"}$	$-\xi_2 B_2^{(b)}$	$\xi_3 B_3^{(b)}$	$\xi_4 B_4^{(b)}$	$\xi_5 B_5^{(b)}$
	0.0165	1.015(12)	0.247(3)	1.877(21)	0.632(7)
0.0080	0.0200	1.029(11)	0.249(2)	1.892(21)	0.641(7)
	0.0250	1.046(11)	0.253(2)	1.912(20)	0.654(7)
	0.0165	1.038(7)	0.252(2)	1.868(12)	0.632(4)
0.0110	0.0200	1.050(7)	0.254(2)	1.883(11)	0.641(4)
	0.0250	1.065(6)	0.257(2)	1.902(11)	0.654(4)

Table 17. Bare $\xi_i B_i^{(b)}$ for $i = 2, \ldots, 5$, as obtained from eq. (4.15), at each combination of the quark mass pair $(a\mu_\ell, a\mu_{``s"})$ and at $\beta = 3.80$.

$\beta = 3.90 \ (24^3 \times 48)a^4$					
$a\mu_\ell = a\mu_{\text{sea}}$	$a\mu_{\text{``}s\text{''}}$	$-\xi_2 B_2^{(b)}$	$\xi_3 B_3^{(b)}$	$\xi_4 B_4^{(b)}$	$\xi_5 B_5^{(b)}$
	0.0150	0.961(7)	0.236(2)	1.848(14)	0.613(5)
0.0040	0.0220	0.991(7)	0.242(2)	1.888(13)	0.635(4)
	0.0270	1.009(7)	0.245(2)	1.911(13)	0.649(4)
	0.0150	0.979(9)	0.240(2)	1.848(20)	0.617(6)
0.0064	0.0220	1.006(9)	0.245(2)	1.887(16)	0.639(5)
	0.0270	1.023(8)	0.249(2)	1.909(16)	0.652(5)
	0.0150	0.987(8)	0.241(2)	1.860(16)	0.624(5)
0.0085	0.0220	1.014(8)	0.246(2)	1.894(15)	0.644(5)
	0.0270	1.030(8)	0.250(2)	1.914(15)	0.657(5)
	0.0150	0.993(12)	0.243(3)	1.861(24)	0.627(8)
0.0100	0.0220	1.019(12)	0.248(3)	1.894(23)	0.647(8)
	0.0270	1.036(12)	0.252(3)	1.915(23)	0.660(8)
$\beta = 3.90 \ (32^3 \times 64)a^4$					
	0.0150	0.953(5)	0.234(1)	1.855(10)	0.615(3)
0.0030	0.0220	0.982(5)	0.240(1)	1.898(9)	0.638(3)
	0.0270	1.000(5)	0.244(1)	1.924(9)	0.653(3)
	0.0150	0.962(6)	0.236(2)	1.831(12)	0.608(4)
0.0040	0.0220	0.992(6)	0.242(2)	1.875(12)	0.632(4)
	0.0270	1.011(6)	0.246(2)	1.901(11)	0.646(4)

Table 18. Bare $\xi_i B_i^{(b)}$ for $i = 2, \ldots, 5$, as obtained from eq. (4.15), at each combination of the quark mass pair $(a\mu_\ell, a\mu_{\text{``}s\text{''}})$ and at $\beta = 3.90$.

$\beta = 4.05 \ (32^3 \times 64)a^4$					
$a\mu_\ell = a\mu_{\text{sea}}$	$a\mu_{\text{``}s\text{''}}$	$-\xi_2 B_2^{(b)}$	$\xi_3 B_3^{(b)}$	$\xi_4 B_4^{(b)}$	$\xi_5 B_5^{(b)}$
	0.0120	0.915(10)	0.227(2)	1.810(17)	0.596(6)
0.0030	0.0150	0.929(9)	0.230(2)	1.837(17)	0.609(6)
	0.0180	0.943(9)	0.232(2)	1.860(16)	0.620(5)
	0.0120	0.931(9)	0.230(2)	1.820(18)	0.605(6)
0.0060	0.0150	0.946(9)	0.234(2)	1.843(17)	0.617(6)
	0.0180	0.960(9)	0.237(2)	1.864(17)	0.628(6)
	0.0120	0.948(9)	0.234(2)	1.842(17)	0.614(6)
0.0080	0.0150	0.962(8)	0.237(2)	1.861(16)	0.625(5)
	0.0180	0.974(8)	0.240(2)	1.8883(16)	0.636(5)

Table 19. Bare $\xi_i B_i^{(b)}$ for $i = 2, \ldots, 5$, as obtained from eq. (4.15), at each combination of the quark mass pair $(a\mu_\ell, a\mu_{\text{``}s\text{''}})$ and at $\beta = 4.05$.

$\beta = 4.20 \ (48^3 \times 96)a^4$					
$a\mu_\ell = a\mu_{\rm sea}$	$a\mu_{\text{``}s\text{''}}$	$-\xi_2 B_2^{(b)}$	$\xi_3 B_3^{(b)}$	$\xi_4 B_4^{(b)}$	$\xi_5 B_5^{(b)}$
	0.0116	0.878(7)	0.219(2)	1.801(13)	0.592(4)
0.0020	0.0129	0.892(7)	0.222(2)	1.830(13)	0.606(4)
	0.0142	0.905(7)	0.225(2)	1.855(14)	0.618(5)
$\beta = 4.20 \ (32^3 \times 64)a^4$					
	0.0116	0.939(20)	0.234(5)	1.831(38)	0.608(12)
0.0065	0.0129	0.950(19)	0.237(5)	1.856(36)	0.628(12)
	0.0142	0.961(18)	0.239(5)	1.877(35)	0.632(12)

Table 20. Bare $\xi_i B_i^{(b)}$ for $i = 2, \ldots, 5$, as obtained from eq. (4.15), at each combination of the quark mass pair $(a\mu_\ell, a\mu_{\text{``}s\text{''}})$ and at $\beta = 4.20$.

E   Results for R_i and B_i

In this appendix we present in detail our results in the $\overline{\rm MS}$ scheme of ref. [15] at $2\,{\rm GeV}$ for the quantities R_i and B_i (cf. eqs. (4.19), (4.20) and eq. (4.18) respectively). We also give the R_i results computed in the indirect way of eq. (5.6). In table 21 we gather results obtained employing M1-type RCs and using ChPT (NLO) fit formula, polynomial and linear fit functions (see eqs. (5.2)–(5.3), and $n = 2$ and $n = 1$ of eq. (5.1) respectively). In table 22 we show the respective results when using M2-type RCs. Instead of using the definition of eq. (4.19), we have employed a slightly different but equivalent one which reads

$$\tilde{R}'_i = \tilde{R}_i \, \frac{[G_K^{34} G_K^{12}]|_{\rm M1}}{[G_K^{34} G_K^{12}]|_{\rm M2}} \tag{E.1}$$

where indices M1 and M2 refer to the use of the respective type of renormalisation constants and we define $G_K^{(12,34)}|_{(M1,M2)} = \langle 0|P^{(12,34)}|K\rangle|_{(M1,M2)}$. We find that the quantity defined in eq. (E.1) has smaller $O(a^2)$ effects.

In figures 11 and 12 we show the combined fit for the ratios, $\tilde{R}'_i$ and bag parameters B_i ($i = 2, \ldots, 5$) against the light quark mass when M2-type RCs are used.

We remark that a good agreement between the continuum limit results for the bag parameters B_i and the matrix elements ratios R_i obtained using M2-type RCs and their counterparts based on M1-type RCs, as we observe for $i = 1, 2, 3, 4$ (for $i = 1$ see also ref. [8]), provides a valuable check of the smallness of residual systematic errors in the evaluation of RI-MOM RCs with the M1-method. In particular possible systematic errors stemming in the M1-method from the inadequacy at non-high momenta ($\tilde{p}^2$) of the perturbative operator anomalous dimensions used in the analysis or from the removal of the leading cutoff effects via a linear fit in $\tilde{p}^2$ are strongly reduced or absent when using the M2-method for RCs. This is so because in this latter approach (see ref. [18] and appendix B) the RCs are extracted from Landau gauge correlators at a rather high $\tilde{p}^2$-value

| Fit	i	R_i	R_i(via eq. (5.6))	B_i
	1	1	1	0.53(2)
	2	-13.7(3)	-15.4(2.2)	0.52(2)
ChPT	3	4.8(2)	5.3(08)	0.89(5)
	4	24.8(6)	28.5(4.2)	0.80(3)
	5	6.4(3)	7.3(1.1)	0.61(4)
	1	1	1	0.53(2)
	2	-14.3(5)	-15.5(2.3)	0.52(2)
Pol	3	4.9(3)	5.3(09)	0.89(7)
	4	24.9(8)	27.8(4.5)	0.78(4)
	5	6.6(5)	7.3(1.3)	0.61(5)
	1	1	1	0.53(2)
	2	-13.7(3)	-15.7(2.2)	0.52(2)
L	3	4.8(2)	5.4(8)	0.90(5)
	4	23.6(6)	27.9(4.1)	0.78(3)
	5	6.1(3)	7.1(1.1)	0.60(4)

Table 21. R_i (direct computation through eq. (4.19) and indirect computation through eq. (5.6)) and B_i results using M1-type RCs for three kinds of fit function, namely a ChPT (NLO) fit, a polynomial and a linear fit with respect to the light quark mass. For $i = 2, 3$ the ChPT (NLO) fit formula for R_i coincides with the linear one (we refer to results of the 3rd column).

(fixed to $\sim 9\,\mathrm{GeV}^2$ for all β's) but comes at the price of generically larger lattice artifacts on the RCs, which we partly suppress by removing the perturbatively known $\mathrm{O}(a^2 g^2)$ contributions. For the case of O_i with $i = 1, 2, 3, 4$ the resulting cutoff effects on R_i and B_i (see figures 11 and 12) appear to be under control and the continuum extrapolation is reliable. On the contrary, the case of B_5 and R_5 (see panel d) of the figures above) is a typical one where too large cutoff effects affecting the M2-type RCs make unreliable the results appearing in the $i = 5$-lines of table 22.

Finally we give our continuum results for B_i and R_i in the $\overline{\mathrm{MS}}$ scheme of Buras et al., defined in ref. [15], and the RI-MOM scheme at $3\,\mathrm{GeV}$, see tables 23 and 24 respectively.

Fit	i	R_i	R_i(via eq. (5.6))	B_i
	1	1	1	0.53(2)
	2	-13.6(2)	-14.9(2.1)	0.50(1)
ChPT	3	4.7(1)	5.1(07)	0.87(3)
	4	24.7(4)	27.5(3.4)	0.77(2)
	5	5.1(2)	6.1(9)	0.51(2)
	1	1	1	0.53(2)
	2	-14.0(4)	-15.0(2.2)	0.50(2)
Pol	3	4.8(2)	5.2(08)	0.87(5)
	4	24.4(7)	26.4(3.9)	0.74(3)
	5	5.2(3)	6.0(9)	0.50(3)
	1	1	1	0.54(2)
	2	-13.6(2)	-15.0(2.1)	0.51(1)
L	3	4.7(1)	5.2(8)	0.88(3)
	4	23.7(4)	26.5(3.5)	0.75(2)
	5	4.9(2)	5.8(9)	0.50(2)

Table 22. R_i (direct computation through eq. (E.1) and indirect computation through eq. (5.6)) and B_i results using M2-type RCs for three kinds of fit function, namely a ChPT (NLO) fit, a polynomial and a linear fit with respect to the light quark mass. For $i = 2, 3$ the ChPT (NLO) fit formula for R_i coincides with the linear one (we refer to results of the 3rd column). The results in the lines corresponding to $i = 5$ here are not reliable, due to very large cutoff effects resulting in this case from the use of M2-type RCs (see text).

$\overline{\text{MS}}$ (3 GeV)				
B_1	B_2	B_3	B_4	B_5
0.51(2)	0.47(2)	0.78(4)	0.75(3)	0.60(3)
R_1	R_2	R_3	R_4	R_5
1	-15.6(5)	5.3(3)	28.6(9)	7.8(4)

Table 23. Continuum limit results for B_i and R_i, renormalized in the $\overline{\text{MS}}$ scheme of ref. [15] at 3 GeV.

RI-MOM (3 GeV)				
B_1	B_2	B_3	B_4	B_5
0.51(2)	0.61(2)	1.02(5)	0.92(4)	0.73(5)
R_1	R_2	R_3	R_4	R_5
1	-14.6(5)	5.0(3)	25.6(9)	6.9(4)

Table 24. Continuum limit results for B_i and R_i, renormalized in the RI-MOM scheme at 3 GeV.
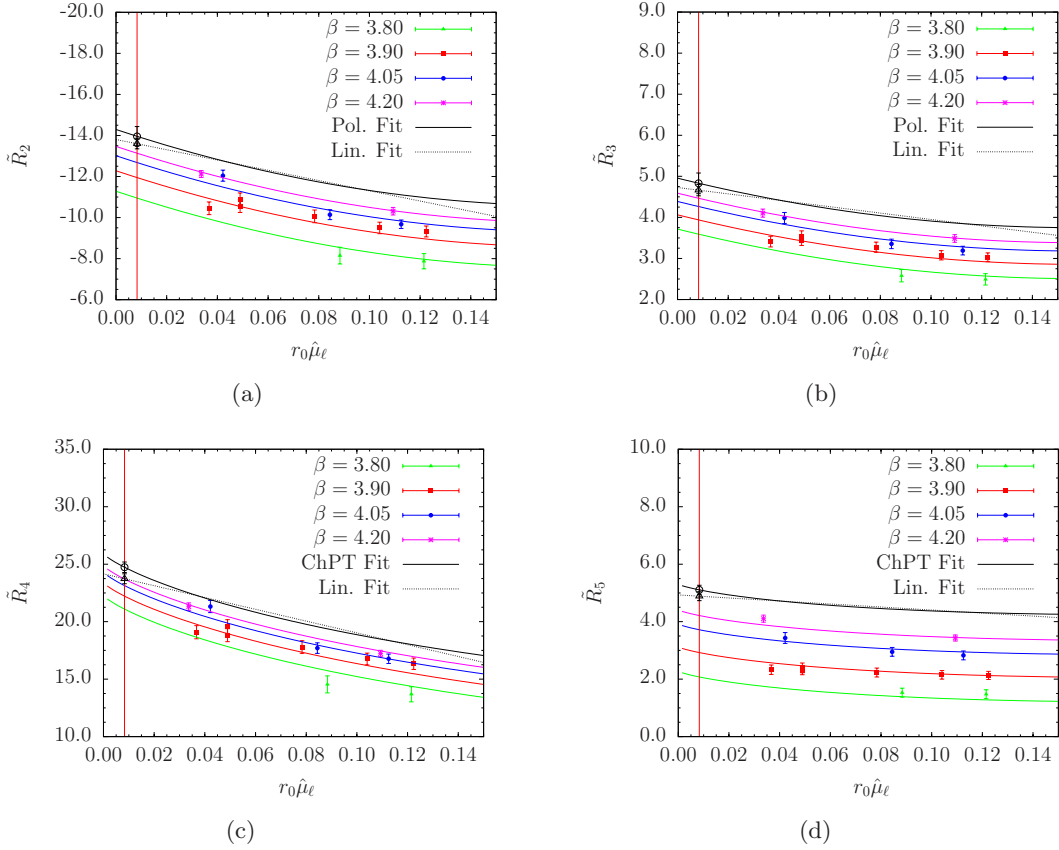
Figure 11. Solid lines in panels (a) and (b) show the behaviour vs. the renormalized light quark mass of the combined chiral and continuum fits (according to the polynomial formula (5.1) with $n = 2$) of the $\tilde{R}_i^{'}$ (see eq. (E.1)), with $i = 2$ and $i = 3$ respectively, renormalized in the $\overline{\text{MS}}$ scheme of ref. [15] at $2\,\text{GeV}$ with the M2-type RCs. The full black line is the continuum limit curve. In panels (c) and (d), solid lines, instead, show the combined chiral and continuum described by NLO-ChPT, eq. (5.3) for $i = 4$ and $i = 5$, respectively. The full black line is the continuum limit curve. The dashed black line represents the continuum limit curve in the case of the linear fit ansatz. Black open circles and triangles stand for the results at the physical point corresponding to the polynomial (panels (a) and (b)) and ChPT fit (panels (c) and (d)), and linear fit ansatz, respectively.
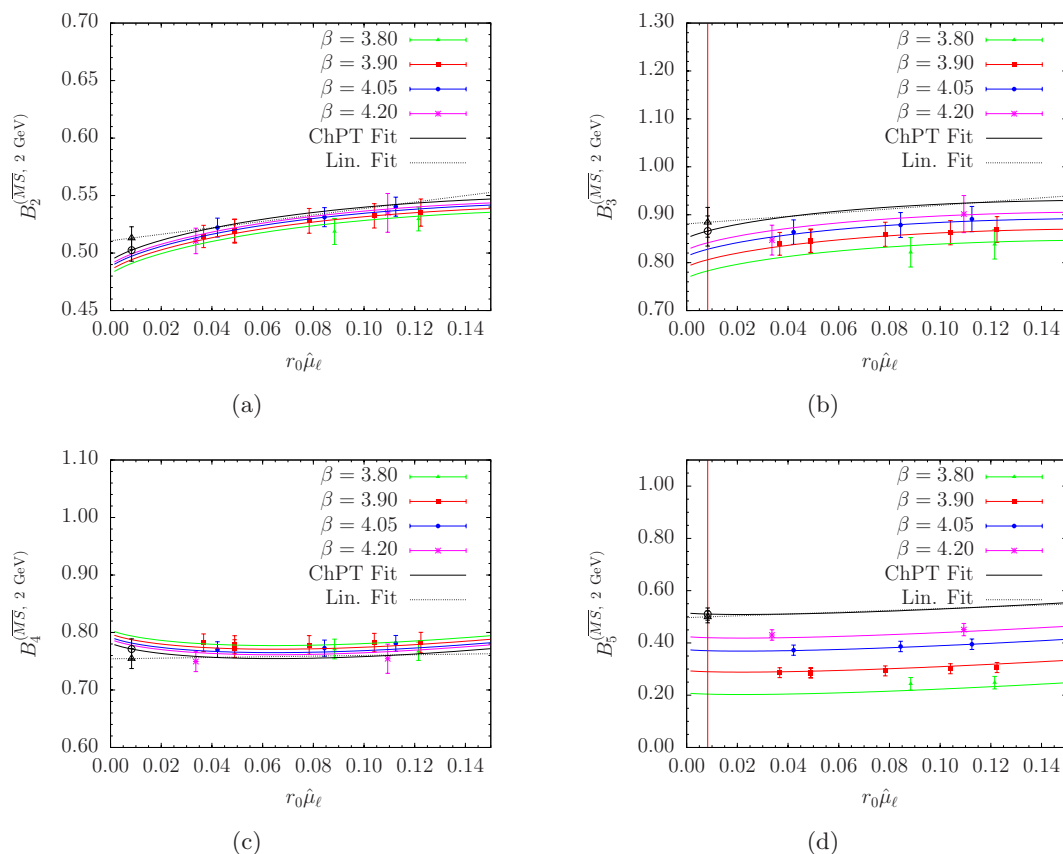
Figure 12. Solid lines in panels (a) to (d) show the behaviour vs. the renormalized light quark mass of the combined chiral and continuum fits (according to the ChPT fit formula (5.2)) for the B_i parameters with $i = 2, \ldots, 5$ respectively, renormalized in the $\overline{\text{MS}}$ scheme of ref. [15] at $2\,\text{GeV}$ with the M2-type RCs. The full black line is the continuum limit curve (5.1). The dashed black line represents the continuum limit curve in the case of the linear fit ansatz. Black open circles and triangles stand for the results at the physical point corresponding to the ChPT fit and linear fit ansatz, respectively.

References

[1] F. Gabbiani, E. Gabrielli, A. Masiero and L. Silvestrini, *A complete analysis of FCNC and CP constraints in general SUSY extensions of the standard model*, *Nucl. Phys.* **B 477** (1996) 321 [hep-ph/9604387] [INSPIRE].

[2] G. Beall, M. Bander and A. Soni, *Constraint on the Mass Scale of a Left-Right Symmetric Electroweak Theory from the K(L) K(S) Mass Difference*, *Phys. Rev. Lett.* **48** (1982) 848 [INSPIRE].

[3] F. Gabbiani and A. Masiero, *FCNC in generalized supersymmetric theories*, *Nucl. Phys.* **B 322** (1989) 235 [INSPIRE].

[4] E. Gabrielli, A. Masiero and L. Silvestrini, *Flavor changing neutral currents and CP-violating processes in generalized supersymmetric theories*, *Phys. Lett.* **B 374** (1996) 80 [hep-ph/9509379] [INSPIRE].

[5] RBC and UKQCD collaborations, P. Boyle, N. Garron and R. Hudspith, *Neutral kaon mixing beyond the standard model with $n_f = 2 + 1$ chiral fermions*, *Phys. Rev.* **D 86** (2012) 054028 [arXiv:1206.5737] [INSPIRE].

[6] A. Donini, V. Giménez, L. Giusti and G. Martinelli, *Renormalization group invariant matrix elements of $\Delta S = 2$ and $\Delta I = 3/2$ four fermion operators without quark masses*, *Phys. Lett.* **B 470** (1999) 233 [hep-lat/9910017] [INSPIRE].

[7] R. Babich et al., *$K^0 - \bar{K}^0$ mixing beyond the standard model and CP-violating electroweak penguins in quenched QCD with exact chiral symmetry*, *Phys. Rev.* **D 74** (2006) 073009 [hep-lat/0605016] [INSPIRE].

[8] ETM collaboration, M. Constantinou et al., *B_K-parameter from $N_f = 2$ twisted mass lattice QCD*, *Phys. Rev.* **D 83** (2011) 014505 [arXiv:1009.5606] [INSPIRE].

[9] UTFIT collaboration, M. Bona et al., *Model-independent constraints on $\Delta F = 2$ operators and the scale of new physics*, *JHEP* **03** (2008) 049 [arXiv:0707.0636] [INSPIRE].

[10] ALPHA collaboration, R. Frezzotti, P.A. Grassi, S. Sint and P. Weisz, *Lattice QCD with a chirally twisted mass term*, *JHEP* **08** (2001) 058 [hep-lat/0101001] [INSPIRE].

[11] R. Frezzotti and G. Rossi, *Chirally improving Wilson fermions. I. O(a) improvement*, *JHEP* **08** (2004) 007 [hep-lat/0306014] [INSPIRE].

[12] R. Frezzotti and G. Rossi, *Chirally improving Wilson fermions. II. Four-quark operators*, *JHEP* **10** (2004) 070 [hep-lat/0407002] [INSPIRE].

[13] J.A. Bagger, K.T. Matchev and R.-J. Zhang, *QCD corrections to flavor changing neutral currents in the supersymmetric standard model*, *Phys. Lett.* **B 412** (1997) 77 [hep-ph/9707225] [INSPIRE].

[14] C. Allton et al., *B parameters for $\Delta S = 2$ supersymmetric operators*, *Phys. Lett.* **B 453** (1999) 30 [hep-lat/9806016] [INSPIRE].

[15] A.J. Buras, M. Misiak and J. Urban, *Two loop QCD anomalous dimensions of flavor changing four quark operators within and beyond the standard model*, *Nucl. Phys.* **B 586** (2000) 397 [hep-ph/0005183] [INSPIRE].

[16] G. Martinelli, C. Pittori, C.T. Sachrajda, M. Testa and A. Vladikas, *A general method for nonperturbative renormalization of lattice operators*, *Nucl. Phys.* **B 445** (1995) 81 [hep-lat/9411010] [INSPIRE].

[17] E. Franco and V. Lubicz, *Quark mass renormalization in the MS-bar and RI schemes up to the NNLO order*, *Nucl. Phys.* **B 531** (1998) 641 [hep-ph/9803491] [INSPIRE].

[18] ETM collaboration, M. Constantinou et al., *Non-perturbative renormalization of quark bilinear operators with $N_f = 2$ (tmQCD) Wilson fermions and the tree-level improved gauge action*, *JHEP* **08** (2010) 068 [arXiv:1004.1115] [INSPIRE].

[19] http://www.utfit.org/UTfit.

[20] M. Misiak, S. Pokorski and J. Rosiek, *Supersymmetry and FCNC effects*, *Adv. Ser. Direct. High Energy Phys.* **15** (1998) 795 [hep-ph/9703442] [INSPIRE]. To appear in *Advanced Series on Directions in High-Energy Physics. Review Volume: Heavy Flavors II*, A.J. Buras and M. Lindner eds., World Scientific, Singapore.

[21] M. Ciuchini, G. Degrassi, P. Gambino and G. Giudice, *Next-to-leading QCD corrections to $B \to X_s \gamma$ in supersymmetry*, *Nucl. Phys.* **B 534** (1998) 3 [hep-ph/9806308] [INSPIRE].

[22] C. Bobeth et al., *Upper bounds on rare K and B decays from minimal flavor violation*, *Nucl. Phys.* **B 726** (2005) 252 [hep-ph/0505110] [INSPIRE].

[23] M. Blanke, A.J. Buras, D. Guadagnoli and C. Tarantino, *Minimal Flavour Violation Waiting for Precise Measurements of $\Delta M_s, S_{\Psi\phi}, A_{SL}^s, |V_{ub}|, \gamma$ and $B_{s,d}^0 \to \mu^+\mu^-$*, *JHEP* **10** (2006) 003 [hep-ph/0604057] [INSPIRE].

[24] A. Buras, P. Gambino, M. Gorbahn, S. Jager and L. Silvestrini, *Universal unitarity triangle and physics beyond the standard model*, *Phys. Lett.* **B 500** (2001) 161 [hep-ph/0007085] [INSPIRE].

[25] G. D'Ambrosio, G. Giudice, G. Isidori and A. Strumia, *Minimal flavor violation: An Effective field theory approach*, *Nucl. Phys.* **B 645** (2002) 155 [hep-ph/0207036] [INSPIRE].

[26] C. Csáki, A. Falkowski and A. Weiler, *The flavor of the composite pseudo-goldstone Higgs*, *JHEP* **09** (2008) 008 [arXiv:0804.1954] [INSPIRE].

[27] C. Aubin, J. Laiho and R.S. Van de Water, *The neutral kaon mixing parameter B_K from unquenched mixed-action lattice QCD*, *Phys. Rev.* **D 81** (2010) 014507 [arXiv:0905.3947] [INSPIRE].

[28] Y. Aoki et al., *Continuum Limit of B_K from $2+1$ Flavor Domain Wall QCD*, *Phys. Rev.* **D 84** (2011) 014503 [arXiv:1012.4178] [INSPIRE].

[29] J. Laiho and R.S. Van de Water, *Pseudoscalar decay constants, light-quark masses and B_K from mixed-action lattice QCD*, PoS(LATTICE 2011)293 [arXiv:1112.4861] [INSPIRE].

[30] S. Dürr et al., *Precision computation of the kaon bag parameter*, *Phys. Lett.* **B 705** (2011) 477 [arXiv:1106.3230] [INSPIRE].

[31] T. Bae et al., *Kaon B-parameter from improved staggered fermions in $N_f = 2+1$ QCD*, *Phys. Rev. Lett.* **109** (2012) 041601 [arXiv:1111.5698] [INSPIRE].

[32] G. Colangelo et al., *Review of lattice results concerning low energy particle physics*, *Eur. Phys. J.* **C 71** (2011) 1695 [arXiv:1011.4408] [INSPIRE].

[33] P. Dimopoulos, $K^0 - \bar{K}^0$ *on the Lattice*, arXiv:1101.3069 [INSPIRE].

[34] J. Laiho, *Light quark physics from lattice QCD*, arXiv:1106.0457 [INSPIRE].

[35] RBC and QKQCD collaborations, J. Wennekers, *Neutral Kaon Mixing Beyond the Standard Model from 2+1 Flavour Domain Wall QCD*, PoS(LATTICE 2008)269 [arXiv:0810.1841] [INSPIRE].

[36] CP-PACS collaboration, Y. Nakamura et al., *Kaon B-parameters for Generic* $\Delta S = 2$ *Four-Quark Operators in Quenched Domain Wall QCD*, PoS(LAT2006)089 [hep-lat/0610075] [INSPIRE].

[37] M. Bochicchio, L. Maiani, G. Martinelli, G.C. Rossi and M. Testa, *Chiral Symmetry on the Lattice with Wilson Fermions*, *Nucl. Phys.* **B 262** (1985) 331 [INSPIRE].

[38] K. Osterwalder and E. Seiler, *Gauge Field Theories on the Lattice*, *Annals Phys.* **110** (1978) 440 [INSPIRE].

[39] P. Dimopoulos, H. Simma and A. Vladikas, *Quenched* B_K-*parameter from Osterwalder-Seiler tmQCD quarks and mass-splitting discretization effects*, *JHEP* **07** (2009) 007 [arXiv:0902.1074] [INSPIRE].

[40] N. Carrasco et al., $K^0 - \bar{K}^0$ *mixing in the Standard Model from* $N_f = 2 + 1 + 1$ *Twisted Mass Lattice QCD*, PoS(LATTICE 2011)276 [arXiv:1111.1262] [INSPIRE].

[41] F. Farchioni et al., *Pseudoscalar decay constants from* $N_f = 2 + 1 + 1$ *twisted mass lattice QCD*, PoS(LATTICE 2010)128 [arXiv:1012.0200] [INSPIRE].

[42] ETM collaboration, S. Dinter et al., *Sigma terms and strangeness content of the nucleon with* $N_f = 2 + 1 + 1$ *twisted mass fermions*, *JHEP* **08** (2012) 037 [arXiv:1202.1480] [INSPIRE].

[43] R. Frezzotti, G. Martinelli, M. Papinutto and G. Rossi, *Reducing cutoff effects in maximally twisted lattice QCD close to the chiral limit*, *JHEP* **04** (2006) 038 [hep-lat/0503034] [INSPIRE].

[44] S.R. Sharpe and J.M. Wu, *Twisted mass chiral perturbation theory at next-to-leading order*, *Phys. Rev.* **D 71** (2005) 074501 [hep-lat/0411021] [INSPIRE].

[45] S. Aoki and O. Bär, *Twisted-mass QCD, O(a) improvement and Wilson chiral perturbation theory*, *Phys. Rev.* **D 70** (2004) 116011 [hep-lat/0409006] [INSPIRE].

[46] ETM collaboration, P. Boucaud et al., *Dynamical twisted mass fermions with light quarks*, *Phys. Lett.* **B 650** (2007) 304 [hep-lat/0701012] [INSPIRE].

[47] ETM collaboration, P. Boucaud et al., *Dynamical Twisted Mass Fermions with Light Quarks: Simulation and Analysis Details*, *Comput. Phys. Commun.* **179** (2008) 695 [arXiv:0803.0224] [INSPIRE].

[48] P. Weisz, *Continuum Limit Improved Lattice Action for Pure Yang-Mills Theory. 1.*, *Nucl. Phys.* **B 212** (1983) 1 [INSPIRE].

[49] ETM collaboration, B. Blossier et al., *Average up/down, strange and charm quark masses with* $N_f = 2$ *twisted mass lattice QCD*, *Phys. Rev.* **D 82** (2010) 114513 [arXiv:1010.3659] [INSPIRE].

[50] D. Becirevic and G. Villadoro, *Remarks on the hadronic matrix elements relevant to the SUSY $K^0 - \bar{K}^0$ mixing amplitude*, *Phys. Rev.* **D 70** (2004) 094036 [`hep-lat/0408029`] [INSPIRE].

[51] A. Donini, V. Giménez, G. Martinelli, M. Talevi and A. Vladikas, *Nonperturbative renormalization of lattice four fermion operators without power subtractions*, *Eur. Phys. J.* **C 10** (1999) 121 [`hep-lat/9902030`] [INSPIRE].

[52] M. Ciuchini et al., *Next-to-leading order QCD corrections to $\Delta F = 2$ effective Hamiltonians*, *Nucl. Phys.* **B 523** (1998) 501 [`hep-ph/9711402`] [INSPIRE].

[53] S. Weinberg, *The quantum theory of fields, I*, Cambridge University Press, Cambridge U.K. (1996).

[54] M. Constantinou, V. Lubicz, H. Panagopoulos and F. Stylianou, *$O(a^2)$ corrections to the one-loop propagator and bilinears of clover fermions with Symanzik improved gluons*, *JHEP* **10** (2009) 064 [`arXiv:0907.0381`] [INSPIRE].

[55] M. Constantinou et al., *Perturbative renormalization factors and $O(a^2)$ corrections for lattice 4-fermion operators with improved fermion/gluon actions*, *Phys. Rev.* **D 83** (2011) 074503 [`arXiv:1011.6059`] [INSPIRE].

[56] K. Chetyrkin and A. Retey, *Renormalization and running of quark mass and field in the regularization invariant and MS-bar schemes at three loops and four loops*, *Nucl. Phys.* **B 583** (2000) 3 [`hep-ph/9910332`] [INSPIRE].